Physics of Fluids

A new kinematic criterion for vortex ring pinch-off

Cite as: Phys. Fluids **33**, 037120 (2021); https://doi.org/10.1063/5.0033719
Submitted: 18 October 2020 . Accepted: 15 February 2021 . Published Online: 19 March 2021

Michael Krieg, and Kamran Mohseni

Physics of Fluids ARTICLE scitation.org/journal/phf

A new kinematic criterion for vortex ring pinch-off

Cite as: Phys. Fluids **33**, 037120 (2021); doi: 10.1063/5.0033719
Submitted: 18 October 2020 · Accepted: 15 February 2021 ·
Published Online: 19 March 2021

View Online Export Citation CrossMark

Michael Krieg[1,a)] and Kamran Mohseni[2]

AFFILIATIONS

[1]Ocean and Resources Engineering, University of Hawaii Manoa, Honolulu, Hawaii 96822, USA
[2]Mechanical and Aerospace Engineering, and Electrical and Computer Engineering, University of Florida, Gainesville, Florida 32611, USA

[a)]Author to whom correspondence should be addressed: kriegmw@hawaii.edu

ABSTRACT

This study lays out a methodology whereby conditions necessary for a vortex ring to separate from the shear flow can be identified by a relationship between characteristic velocities of the jet and the vortex ring along the axis of symmetry. This criterion identifies pinch-off to take place when the velocity induced at the origin of the forming vortex ring surpasses the maximum feeding velocity along the centerline, defined to be twice the piston velocity. A strategy for determining these characteristic velocities purely from the jet driving programs (i.e., without direct knowledge of the state of the leading vortex ring) is presented. A variety of jet driving conditions, including different nozzle geometries (converging radial velocity) and different jet velocity programs, are examined to validate the relationship between pinch-off and the characteristic velocities. These parameters are examined and adjusted independently of each other so that the effect of each jetting parameter can be observed independently. Nozzles which induce a converging radial velocity decrease the jet formation number to approximately two (for nearly constant velocity programs), due to the large increase in vorticity flux without increasing volume flux. Accelerating the jet velocity to compensate for the growing vortex ring substantially increases the formation number of both parallel and converging jet flows. The new centerline velocity criterion coincided very closely with vortex ring pinch-off for all cases tested, validating this criterion as a predictive tool.

I. INTRODUCTION

One of the most well studied and denotative aspects of vortex ring formation is a phenomenon commonly referred to as "pinch-off." This is a process where a forming vortex ring achieves a critical state and separates from the remainder of the shear flow feeding the vortex ring's growth. This phenomenon gained notoriety from a classic paper by Gharib *et al.*[1] In that study, vortex rings were generated experimentally using a piston-cylinder device and analyzed using digital particle image velocimetry (DPIV). It was observed that as fluid continues to be ejected, the primary vortex ring grows until it reaches a critical state and can no longer accept circulation in its current arrangement, and "pinches off" from the trailing shear flow. It was observed that this phenomenon is closely related to a dimensionless timescale termed the formation time. The formation time is a measure of the time since initiation of the flow normalized by the piston velocity, u_p, and a characteristic length scale. Formation time is defined by Gharib *et al.*[1] to be

$$t^* = \frac{\int_0^t u_p \, d\tilde{t}}{D}, \tag{1}$$

where D is the nozzle diameter, which is the characteristic length scale for jets with static nozzles, and $\tilde{t}$ is just a dummy variable for time t. A circulation history of both the vortex ring and the total expelled jet was extracted from the DPIV vorticity field. Gharib *et al.* defined the formation number (which will be referred to by τ in this paper) as the formation time when the total jet circulation first reached the final circulation of the separated vortex ring, and additionally showed that jets generated with a variety of piston velocity programs, $u_p(t)$, have a nearly universal formation number falling between 3.6 and 4.2 for all cases. However, more recent studies have called into question the universality of the formation number as will be described shortly.

Vortex ring pinch-off is known to play an important role in an abundance of both engineered and biological jet flows. The formation number indicates a fundamental shift in the efficiency of squid and jellyfish locomotion,[2–8] and the nature of vortex ring formation serves as a good indicator for cardiac health.[9] Additionally, biologically inspired pulsatile jet thrusters are observed to suffer losses when operating at high frequencies with stroke ratios above the formation number.[10]

Therefore, understanding the physical mechanisms behind ring pinch-off and being able to predict when it will occur while enhance our understanding of jetting in multiple fields. Vortex rings in general can be categorized based on the "thickness" of the vortex core relative to the overall size of the ring.[11,12] At one end of the spectrum is a vortex ring which is confined to a circular vortex filament. As the thickness of the core increases relative to the toroidal radius, the core area begins to shift from being perfectly circular to being weighted at the edge closest to the ring's central axis. A hypothetical maximum core area is reached at the other end of the spectrum with Hill's spherical vortex, whose core area cross section is a semicircle with the straight edge lying on the axis of symmetry.[13] As formation time increases for a jet flow, the forming vortex ring at the leading edge grows with its core area increasing relative to the overall size of the vortex ring. Analysis by Mohseni and Gharib[14] showed that the universal timescale for pinch-off observed in Ref. 1 does not correspond to Hill's spherical vortex suggesting a limitation in piston-cylinder vortex generators at creating "thick" vortex rings. They suggested that the formation number could be increased using a vortex generator that creates more energy in the jet for the same impulse and circulation, which could be accomplished by a vortex generator with a variable diameter nozzle or accelerating velocity program.

The experimental studies of Gharib *et al.*[1] were limited to starting flows with a fairly specific jet velocity profile (variation of velocity in the jet flow with respect to radial position), despite the wide range of piston velocity programs. Numerical simulations performed by Rosenfeld *et al.*[15] were not restricted by the limitations of a physical vortex generator, and examined formation dynamics of jets with a wide variety of axial velocity profiles, ranging from the top hat profile to the fully developed Poiseuille flow. It was observed that jets formed with a more parabolic velocity profile separate at a lower formation number, dropping as low as $\tau = 0.9$ for a fully developed pipe flow, demonstrating that τ can be altered by jet flow characteristics. However, all cases were limited to parallel starting jets, meaning that at the entrance boundary there is no radial velocity and the streamlines are parallel (similar to flows created with piston-cylinder vortex generators). The rate of circulation added to the system was observed to be drastically different for non-parallel jet flows,[16] and vortex rings created from converging jet flows have formation numbers substantially lower than parallel jets.[17]

Starting jet vortex ring formation was also examined by Mohseni *et al.*[18] in a numerical simulation where the starting jets (vortex rings) were generated by applying non-conservative forces to the fluid directly in the equations of motion, rather than a prescribed set of velocity profiles at the jet origin boundary. It was shown that the non-dimensional energy of the final vortex ring, which is inversely related to relative vortex core thickness, could be decreased if the shear layer was generated by expanding or accelerated forcing. Vortex rings generated with a background co-flow were studied by Krueger *et al.*,[19] exhibiting a decrease in formation number which was directly proportional to the ratio of jet velocity to co-flow velocity. Dabiri and Gharib[20] present experimental data indicating an increase in formation number as high as $\tau = 8$ for a converging nozzle diameter, but do not directly account for the coupled acceleration of the shear layer. A number of studies have also looked into vortex ring formation in positively[21] and negatively[22] buoyant starting jets. Negatively buoyant jets produce interesting behavior; whereby, as the density differential increases so does the formation number and ring thickness,[22] and the vortex ring attains a maximum penetration depth.[23,24] Eventually the penetration depth becomes very small and there is no clear vortex ring separation.[25]

Several studies have also tried to identify the underlying physical causes of vortex ring pinch-off. It follows from the Kelvin–Benjamin variational principle that the energy of steadily translating vortex rings is maximized with respect to impulse preserving iso-vortical perturbations.[26–28] Gharib *et al.*[1] suggested that pinch-off is a direct manifestation of this principle whereby the energy required for the jet to attain steady motion increases with increasing impulse and circulation until it becomes equal to the jet energy and the vortex ring separates from the remainder of the shear flow. Mohseni and Gharib[18] analytically solved for the formation number utilizing this principle by equating the forming vortex ring to a member of the Norbury family of vortex rings,[11,12,29,30] and using the 1D slug approximation to model the circulation, impulse, and energy of the ejected jet.

Shusser and Gharib[31] suggest that an equality between jet velocity and vortex ring translational velocity should provide a good criterion for vortex ring pinch-off, and equated this condition to the Kelvin–Benjamin variational principle in Ref. 32. This analysis represented the Kelvin–Benjamin principle by the constraint that the required energy for steady propagation must be less than the jet energy or the vortex ring will pinch-off. This reduces to the constraint that the non-dimensional energy, $\alpha = E/\Gamma^{3/2}I^{1/2}$ (where E is the kinetic energy of the ring, Γ is the circulation, and I is the impulse[1,14,33]), must be greater than some constant of proportionality, $\alpha \geq A$, and the constant, A, is heuristically assigned the value 0.33 which was seen to be the limiting the non-dimensional energy of vortex rings in Ref. 1. From a predictive standpoint, this criterion is no more useful than the constrain $L/D \lesssim 3.8$, and in fact for parallel jets expelled with constant piston velocity, these criteria are identical since $\alpha \approx \sqrt{\pi/2}(L/D)^{-1}$ for that case. Furthermore, using a limiting non-dimensional energy to define pinch-off makes the assumption that all vortex rings created from starting jets will have the same non-dimensional energy, corresponding to a maximum core thickness well below that of the theoretical maximum. However, vortex rings with non-dimensional energy below this heuristic limit have been formed in simulation by expanding the diameter of or accelerating the jet flow[18] and have been formed experimentally with jets ejected through large aspect ratio slits.[34] Therefore, a limiting non-dimensional energy cannot be used as an effective tool in predicting pinch-off.

This study re-evaluates the kinematic pinch-off criterion presented by Shusser and Gharib[32] and proposes another more robust criterion. This study also provides additional experimental data on the formation number of converging jets to support the simulations of Rosenfeld *et al.*[17] and extends pinch-off criterion analysis to non-parallel starting jets. The paper also explicitly investigates the validity of this new pinch-off criterion in cases where the jet forms a stable vortex ring with non-dimensional energy well below the $\alpha \geq 0.33$ limit. Section II presents the general jet modeling scheme and clearly defines both pinch-off criteria. The experimental setup is described in Sec. III.

Section IV presents the experimental results; more specifically, the validity of multiple velocity approximations is presented in Sec. IV A, and Sec. IV B contains the formation number analysis for various jets.

II. FORMULATION

Consider a starting jet flow as depicted in Fig. 1. The inherent symmetry of the problem lends toward a cylindrical coordinate system with positions r in the radial direction, x in the axial direction, at an angle ϕ about the x-axis, and velocity vector $\vec{u} = [v, w, u]^T$. The flow is assumed to be perfectly axisymmetric, $\partial/\partial\phi = 0$, with no swirl $w = 0$. The fluid in the domain is assumed to start at rest, and a jet flow is initiated at the entrance plane, $x = 0$, at time $t = 0$. We define the piston velocity to be the volume flux across the nozzle exit plane, $\forall$, over the nozzle area, $u_p = \forall / \pi R^2$, where R is the nozzle radius. This definition is independent of the mechanism used for jet pulsation.

A. Necessary conditions for pinch-off

In this section, the physical mechanism of vortex ring pinch-off is briefly described as well as a methodology for predicting when the pinch-off will take place for any general starting jet flow. Consider a starting jet flow which is still attached to the leading vortex ring as depicted in Fig. 1. The shear tube, which extends into the domain with the jet flow, coils up at the free end starting the vortex ring formation process. As the vortex ring grows, the self-induced velocity on the spiraling shear layer increases, approaching the feeding velocity of the starting jet. When the induced velocity surpasses the feeding velocity, the trailing shear tube becomes unstable, and the shear layer crossing the vortex boundary (vortex bubble) is driven toward the axis of symmetry under the induction of the vortex ring. Vorticity cancelation at the axis of symmetry causes the shear layer in this region to break, separating the primary vortex ring from the trailing shear layer. Vorticity cancelation at the axis of symmetry was observed to be typical for thick vortex rings in Ref. 18. The free end of the trailing shear layer rolls into a secondary vortex ring and the primary vortex ring settles upon a stable arrangement. The primary vortex ring quickly travels downstream out of range of the influence of the secondary slower moving vortex ring, and the evolution of the ring becomes only dependent on viscosity (refer to the work of Maxworthy[35,36]). This process is depicted graphically in Fig. 2 where a diagram of the shear layer is shown alongside actual vorticity contours at several representative times during pulsation.

In order to model this process and predict jet formation number for various driving conditions, we need to define a criterion which coincides with the shear layer instability. Similar to the work of Shusser and Gharib,[32] we will use the relationship between a characteristic feeding velocity and a characteristic vortex ring velocity to define this criterion; however, the important quantities will be treated very differently and our analysis will not be restricted to specific nozzle configurations, piston velocity programs, or nozzle radius programs. The model of Shusser and Gharib suggested that an appropriate criterion for vortex ring pinch-off is when the propagation or translational velocity of the primary vortex ring, U_{tr}, surpasses the jet velocity driving the flow, making corrections to the jet velocity based on

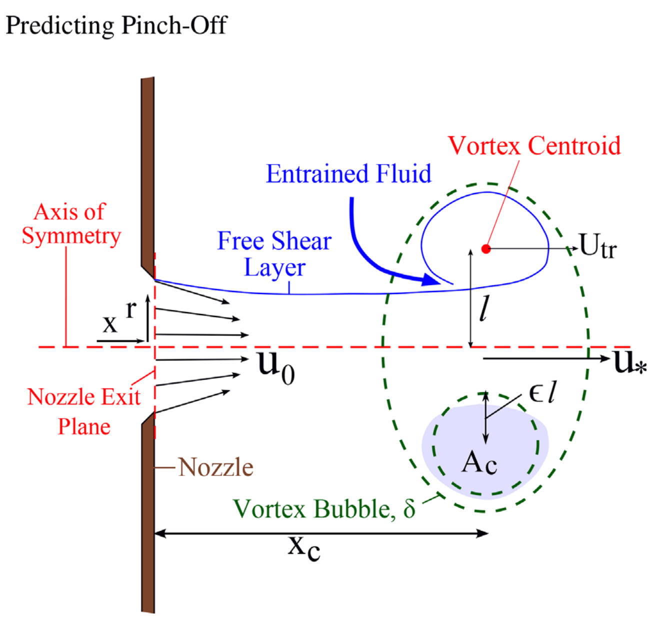

FIG. 1. Diagram of vortex ring formation and important flow characteristics.

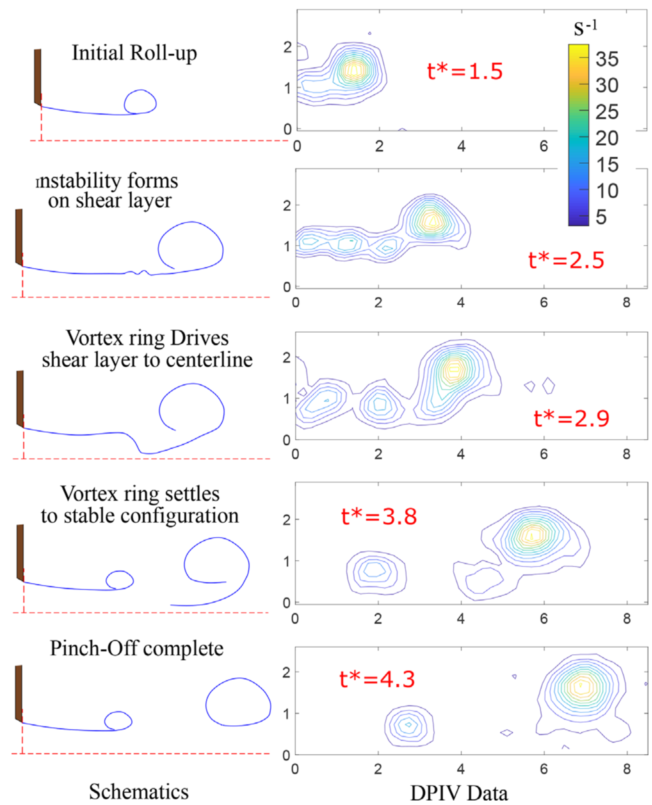

FIG. 2. At several characteristic times during pulsation, the evolution of the shear layer is represented schematically on the left and actual corresponding vorticity contours are shown to the right. The time is marked by the dimensionless formation time. The vorticity contours were taken from a converging jet with a stroke ratio $L/D = 2.4$, and piston velocity of $u_p \approx 7$ cm/s.

conservation of mass flux. We will refer to this as the SG (Shuser–Gharib) criterion throughout this manuscript. We will demonstrate that this criterion does not exactly coincide with vortex ring pinch-off because the translational velocity is considerably lower than the velocity induced at the location where the shear tube interacts with the forming vortex ring and shows that other choices for the characteristic vortex ring velocity are more appropriate. Alternatively, a velocity criterion is proposed here which compares jet feeding velocity to the velocity induced by the forming vortex at the axis of symmetry, where separation of the shear tube occurs.

Here it should be noted that vortex ring pinch-off is not an instantaneous event. Rather, it is a dynamic process whereby the leading vortex ring eventually settles upon a stable configuration. The "instant" associated with pinch-off can only be determined by equating the circulation of the final stable ring to the time during formation with equivalent circulation. Therefore, in order to define a criterion corresponding to an instant where the feeding shear flow becomes destabilized, we will similarly compare the dynamically evolving ring/jet flow to an equivalent settled vortical distribution. If a leading vortex ring is allowed to settle, the resulting ring configuration can be uniquely defined by the total circulation, impulse, and kinetic energy. The velocities induced by this stable configuration will provide a maximum velocity that can be achieved in the forming ring if the entire jet was entrained within and provides an accurate characteristic ring velocity up until pinch-off. The total circulation, impulse, and energy of the jet flow can be calculated from the jet driving velocity and nozzle geometry, and will be used as an equivalent stable vortex ring, from which the characteristic vortex ring velocity will be determined.

Since the fluid is assumed to be incompressible, inviscid, and axisymmetric, the rate at which circulation, hydrodynamic impulse, and kinetic energy are created in the jet can be described in terms of the jet velocity profiles along the entrance boundary (nozzle exit plane). A method for determining these quantities was described in great detail by Krieg and Mohseni,[16] and therefore we will only summarize the results here. The total rates of circulation, impulse, and energy added to the system, as well as the pressure distribution along the entrance plane are given by

$$\frac{d\Gamma}{dt} = \frac{1}{2}u_0^2 + \int_0^{R_\infty} u\frac{dv}{dx}\,dr, \tag{2a}$$

$$\frac{dI}{dt} = \rho\pi\int_0^{R_\infty}\left(2u^2 r + u\frac{dv}{dx}r^2 - v^2 r\right)dr, \tag{2b}$$

$$\frac{dE}{dt} = \rho\pi\int_0^{R_\infty}\left(u^2 + v^2 + \frac{2P}{\rho}\right)ur\,dr, \tag{2c}$$

$$P(r) = P_\infty - \frac{\rho}{2}v(r)^2 + \rho\int_r^{R_\infty} u\frac{\partial v}{\partial x} + \frac{\partial v}{\partial t}\,dr, \tag{2d}$$

where Γ, I, and E are the total circulation, impulse, and energy of the jet, P, is the local pressure along the nozzle exit plane, P_∞ is the stagnation pressure, u_0 is the axial jet velocity at the axis of symmetry, and the surface integrals are all evaluated along the entrance plane ($x = 0$). If we make the standard slug model approximation, meaning that the jet is assumed to have a uniform axial velocity [$u(r) = u_p$ for $0 \le r < R$] and the radial velocity is assumed to be zero, then Eqs. (2) can be drastically simplified,

$$\frac{d\Gamma}{dt_{1D}} = \frac{1}{2}u_p^2, \tag{3a}$$

$$\frac{dI}{dt_{1D}} = \rho\pi u_p^2 R^2, \tag{3b}$$

$$\frac{dE}{dt_{1D}} = \frac{\rho\pi}{2}u_p^3 R^2. \tag{3c}$$

It was observed that the radial velocity profile as well as the radial velocity gradient of jets ejected through orifice nozzles (orifice nozzles consist of a flat plate with a central circular orifice) can be approximated adequately by a linear profile, $v = k_1 r$, $\partial v/\partial x = k_2 r$ (Krieg and Mohseni[16]). Taking this approximation for the radial velocity profile and again assuming a uniform axial velocity profile Eqs. (2) become

$$\frac{d\Gamma}{dt_{2D}} = \frac{1}{2}u_p^2\left(1 + k_2^*\right), \tag{4a}$$

$$\frac{dI}{dt_{2D}} = \frac{\rho\pi}{4}u_p^2 R^2\left(4 + k_2^* - k_1^{*2}\right), \tag{4b}$$

$$\frac{dE}{dt_{2D}} = \frac{\rho\pi}{4}u_p^3 R^2\left(2 + k_2^*\right), \tag{4c}$$

where k_1^* and k_2^* are the radial slopes normalized by the piston velocity and nozzle radius, $k_1^* = k_1 R/u_p$, $k_2^* = k_2 R^2/u_p$.

Next the bulk jet quantities, Γ, I, and E, will be equated to properties of stable vortex rings to allow a direct comparison of characteristic feeding and vortex ring velocities.

The translational velocity of the vortex ring, U_{tr}, was used as the characteristic vortex ring velocity for the SG criterion; however, the local velocity anywhere within the toroidal radius will be significantly higher than this propagation velocity, with the exception of extremely thin core vortex rings. The velocity along the shear layer at the interface between the vortex ring and the driving jet flow, which is at the vortex bubble shown in Fig. 1, is most directly related to the development of instability in the shear layer. Unfortunately, the boundary of the forming vortex ring (vortex bubble) is poorly defined, and a location where the vortex ring ends and the shear flow begins is next to impossible to define, if it even exists. However, at the time when the vortex ring separates, the shear layer has moved very close to the axis of symmetry; therefore, we will define the characteristic feeding velocity as the axial velocity on the centerline produced by the jet flow (ignoring roll-up) and define the characteristic vortex ring velocity as the velocity on the centerline induced by the developing vortex ring.

When the vortex ring pinches off, as was previously mentioned, the shear flow will have been driven toward the axis of symmetry and at some axial location slightly behind the ring origin $u_* = u(r = 0, x = x_c)$ (see Fig. 1), the shear layer will spiral upwards into the forming ring. The instability in the shear layer leading to vorticity cancellation will take place at this location near the axis just behind the origin. Thus, the velocity at the vortex origin is chosen as the characteristic induced velocity. The velocity profile along the axis of symmetry in the vicinity of a vortex ring can be determined from the Stokes stream function, Ψ. For any axisymmetric vorticity distribution, with vorticity confined to the region A_c, the stream function is defined as[37,38]

$$\Psi(r,x) = \frac{1}{2\pi}\int_{A_c}\omega'(r_1 + r_2)[K(\lambda) - E(\lambda)]\,d\vec{x}'. \tag{5}$$

Here the stream function is evaluated at point $\vec{x} = [r, 0, x]^T$; $\vec{x}' = [r', 0, x']^T$ is a dummy position specifying the location of integration, ω' is the vorticity at $\vec{x}'$, K and E are the complete elliptic integrals of the first and second kind, λ is the modulus of the elliptic integrals defined as $\lambda = (r_2 - r_1)/(r_2 + r_1)$, and r_2 and r_1 are distances defined as $r_2 = [(x - x')^2 + (r + r')^2]^{1/2}$ and $r_1 = [(x - x')^2 + (r - r')^2]^{1/2}$. The axial velocity field is then, by definition of the stream function,

$$u(r, x) \equiv \frac{1}{r}\frac{\partial \Psi}{\partial r} = \frac{1}{2\pi}\int_{A_c} \frac{\omega'}{r}(A + B), \tag{6}$$

where

$$A = \left[\frac{r - r'}{r_1} + \frac{r + r'}{r_2}\right][K(\lambda) - E(\lambda)],$$

$$B = \frac{2\left(\dfrac{\partial K}{\partial \lambda} - \dfrac{\partial E}{\partial \lambda}\right)}{r_2 + r_1}\left[\frac{r_1}{r_2}(r + r') - \frac{r_2}{r_1}(r - r')\right].$$

There is an infinite series representation of the elliptic integrals K and E, centered about $\lambda = 0$, which is presented in the following form by Gradshteyn and Ryzhik:[39]

$$K = \frac{\pi}{2}\left\{1 + \left(\frac{1}{2}\right)^2 \lambda^2 + \cdots + \left[\frac{(2n-1)!!}{2^n n!}\right]^2 \lambda^{2n} + \cdots\right\}, \tag{7a}$$

$$E = \frac{\pi}{2}\left\{1 - \frac{1}{4}\lambda^2 - \cdots - \left[\frac{(2n-1)!!}{2^n n!}\right]^2 \frac{\lambda^{2n}}{2n-1} - \cdots\right\}. \tag{7b}$$

In this equation !! represents the double factorial operator. This is a convenient expansion when analyzing behavior at the axis of symmetry because at $r = 0$, the modulus of the elliptic integrals is also zero, $\lambda = 0$, which means that the elliptic integrals evaluated at this location are, $K(0) = E(0) = \pi/2$. The form of (7) allows us to exactly calculate the mth order derivative of the elliptic integrals at the axis of symmetry

$$\left.\frac{\partial^m K}{\partial \lambda^m}\right|_{r=0} = \begin{cases} 0 & \text{if} \quad m = \text{“odd”} \\ m!\left[\dfrac{(m-1)!!}{2^{m/2}\dfrac{m}{2}!}\right]^2 & \text{if} \quad m = \text{“even”} \end{cases}, \tag{8a}$$

$$\left.\frac{\partial^m E}{\partial \lambda^m}\right|_{r=0} = \begin{cases} 0 & \text{if} \quad m = \text{“odd”} \\ \dfrac{m!}{m-1}\left[\dfrac{(m-1)!!}{2^{m/2}\dfrac{m}{2}!}\right]^2 & \text{if} \quad m = \text{“even”} \end{cases}. \tag{8b}$$

The quantities A and B in (6) are equal to zero at the axis of symmetry which makes the fractions A/r and B/r undefined. Therefore, by L'Hopital's rule,

$$u(0, x) = \frac{1}{2\pi}\int_{A_c} \omega'\left(\left[\frac{\partial A}{\partial r}\right]_{r=0} + \left[\frac{\partial B}{\partial r}\right]_{r=0}\right) dx'dr'. \tag{9}$$

The first derivative term, $\partial A/\partial r$, is equal to zero when evaluated at the axis of symmetry. Incorporating (8) the second derivative term can be shown to be equal to $\partial B/\partial r = \pi r'^2/r_1^3$, which means that the velocity profile along the axis of symmetry induced by the vortex ring is

$$u(0, x) = \frac{1}{2}\int_{A_c} \omega' \frac{r'^2}{\left[(x - x')^2 + r'^2\right]^{3/2}} dr'dx'. \tag{10}$$

For the point vortex (zero cross sectional area), the velocity profile becomes very simple

$$u(0, x) = \frac{\Gamma_c}{2}\frac{l^2}{\left[(x - x_c)^2 + l^2\right]^{3/2}} \tag{11a}$$

and

$$u_* = u(0, x_c) = \frac{\Gamma_c}{2l}. \tag{11b}$$

The point vortex (and other thin core vortex rings) has a well-defined toroidal radius,[37,38] $l = \sqrt{I_c/\rho\pi\Gamma_c}$, so that an approximation for the induced velocity can be made in terms of the vortex ring circulation and impulse

$$u_* = \sqrt{\frac{\rho\pi\Gamma_c^3}{4I_c}}. \tag{12}$$

There are a few points to be noted about the previous approximations and simplifications. The jet flow is compared to an equivalent vortex ring so that the characteristic induced velocity can be calculated from total jet circulation and impulse, and that vortex was approximated as a point vortex. The forming vortex ring will certainly have a core with substantial thickness. However, a point vortex ring and thick cored ring with identical circulation and impulse have nearly identical axial velocity at the origin, u_*, but induced velocities vary between the two moving away from that location. Hence Eq. (12) provides good accuracy for calculating velocity at the origin of thick cored vortex rings, as will be shown later in Sec. IV. Furthermore, for thick-cored vortex rings the velocity along the axis of symmetry remains relatively constant across the width of the core; therefore, the velocity induced at the origin will still be very close to the induced velocity at the location where the shear layer becomes destabilized.

Finally, the characteristic feeding velocity is defined as the maximum possible velocity on the centerline due to the jet flow without any shear layer roll-up. The forming vortex ring creates a low pressure zone that helps to draw in the feeding shear layer, so this flow will become more developed increasing the centerline velocity to accommodate the accelerating ring, until it reaches a critical point where the centerline velocity can no longer increase without the shear layer becoming destabilized. In the absence of roll-up, this maximum achievable velocity is that of a fully developed pipe flow (Poisueille flow), which has a centerline velocity which is twice the average velocity, giving a characteristic feeding velocity of $2u_p$.

Under this methodology, the characteristic feeding velocity is directly determined from the driving program, $u_p(t)$, and the characteristic vortex ring velocity is determined by the bulk flow quantities, which are related to the driving programs via (4). This centerline velocity criterion predicts that pinch-off will occur when the characteristic velocity of the growing ring reaches the feeding velocity

$$\sqrt{\frac{\rho\pi\Gamma_c^3}{4I_c}} \geq 2u_p. \tag{13}$$

The SG velocity criterion predicts that pinch-off occurs when the propagation velocity surpasses the corrected jet velocity,[31] which can be written as

$$U_{tr} \geq \left(\frac{R}{l}\right)^2 u_p. \tag{14}$$

For the SG criterion the feeding velocity is scaled by the ratio of vortex ring area to nozzle area in accordance with the conservation of momentum, and U_{tr} will be determined from the motion of the vortex centroid. Both criteria suggest that for a given vortex ring configuration, the pinch-off can be delayed by accelerating piston velocity for a given critical configuration.

In order to calculate the induced velocity, u_*, at any time for an arbitrary velocity program, $u_p(t)$, and thus use this criterion as a means to predict pinch-off, k_1^* and k_2^* in Eq. (4) must be known. These parameters can, for the most part, be set according to the geometry of the nozzle being used. The parameters k_1^* and k_2^* which characterize the amount of converging radial velocity in the jet flow were measured from DPIV data in Ref. 16 for different nozzle geometries and jet velocity programs. These parameters can often be treated as a constant that only changes with nozzle geometry. It was observed that an orifice nozzle produced a consistent converging radial velocity so that the parameters could be considered constant, $k_1^* \approx -0.41$ and $k_2^* \approx 1.05$. For the tube nozzle the forming vortex ring induces a converging radial velocity on the jet flow at the onset which diminishes as the ring develops and moves away from the nozzle. For low stroke ratio jets, the induced radial velocity at the inlet can have a significant effect, but for large stroke ratios (as is the case for jets experiencing pinch-off), the induced radial velocity is small when averaged over the total duration and the radial slope parameters can be approximated, $k_1^* \approx 0$ and $k_2^* \approx 0.25$. These approximate values will be seen to be fairly representative of the cases examined here, as summarized in Table II.

The formation number can be predicted from (13) if the circulation and impulse of the forming vortex ring are known. By this methodology we approximate that up until pinch-off the entire jet is part of the forming vortex ring, so the ring impulse and circulation are equal to the total impulse and circulation expelled in the jet. If we assume that the piston velocity is constant, then at any time, t, the total impulse and circulation are the product of that time and the rates given in (4). Substituting the total jet values into (13) and setting the two sides equal to each other, we can solve for the exact time when the induced velocity, u_*, surpasses the maximum stable feeding velocity, $2u_p$. Appropriately scaling this time by the nozzle diameter and piston velocity yields a prediction for formation time

$$\tau = t^*|_{2u_p=u_*} = \left[\frac{8\left(4 + k_2^* - k_1^{*2}\right)}{\left(1 + k_2^*\right)^3}\right]^{1/2}. \tag{15}$$

Using the approximations for k_1^* and k_2^* just listed, Eq. (15) predicts a formation number of 4.2 for parallel jets and 2.2 for converging jets. Parallel jets are known to have a formation number close to 4 validating this prediction when using tube nozzles, and a formation number of 2.2 will be shown to be a reasonable prediction of the formation number for converging jets with constant velocity.

For jets with more complicated velocity programs, the integrals for impulse and circulation (4) become more complex so that τ cannot be expressed as concisely as (15), but the methodology remains the same. Furthermore, the methodology can also handle jets with any hypothetical velocity profile at the nozzle exit, if that profile is known, by calculating the jet impulse and circulation with the more general (2).

III. EXPERIMENTAL METHODS

To further investigate vortex ring formation dynamics, and to validate the novel kinematic pinch-off criterion, we created experimental starting jet flows with a highly adaptable vortex ring generator and measured the flow field through DPIV throughout the evolution of the jet. This section describes the apparatus and experimental procedures.

A. Vortex generator

The vortex generator used to create the jet flows in this investigation consists of a sealed off canister submerged in a fluid reservoir. The vortex generator has an internal cavity with an oscillating plunger to move fluid in or out of the cavity. The jet actuator has the ability to independently control the jet velocity and nozzle radius during pulsation and can operate at pulsation frequencies from fractions of Hertz up to, and including, frequencies which result in cavitation. The basic layout and different nozzle arrangements are illustrated in Fig. 3. Here we utilize multiple nozzle configurations which can be separated into either static or variable diameter nozzles.

There are two basic types of static nozzles that are used in this study. Jet flows which leave the nozzle with nearly parallel streamlines (no radial velocity) are created using a tube nozzle, which is a long tube connected to the end of the cavity. The tube is sufficiently long, $>6D$, to ensure a 1D flow at the exit prior to ejection. The outside of the tube is tapered at the exit with an angle, γ, as shown in Fig. 3. The tube nozzle is fabricated with a very small γ, very close to 11°. Converging starting jets are created with an orifice nozzle which is simply a flat plate with a central circular orifice. The converging internal streamlines persist downstream creating the converging jet flow. The orifice nozzle is fabricated out of a thin sheet metal, such that the thickness is less than 5% of the orifice diameter and the edge can be considered sharp. It should be noted that both the vortex generator and the nozzles used to generate different jet flow for this study are identical to the system used in Ref. 16 to validate the modeling in Eqs. (2)–(4). The vortex generator is also equipped with a variable diameter nozzle, capable of dynamically changing opening diameter during the jetting process. The changes in diameter were not significant enough to have a measurable effect on formation number, but we have included results and analysis of these trials in the Appendix for the interested reader.

B. DPIV testing

The experimental setup for this research is depicted in Fig. 4. This testing facility consists of a large (2.6 kl) fluid reservoir with visual access from all directions. An outer steel frame supports the fluid container and provides central mounting structures for the vortex generator.

The flow visualization apparatus is composed of a high speed camera and illumination hardware. As depicted in Fig. 4, a 2D cross section of the flow is illuminated with a laser sheet. The flow is seeded with reflective particles 50 μm in diameter (manufactured by Dantec Dynamics). The laser sheet is generated by a 1 W 532 nm laser (Aixis

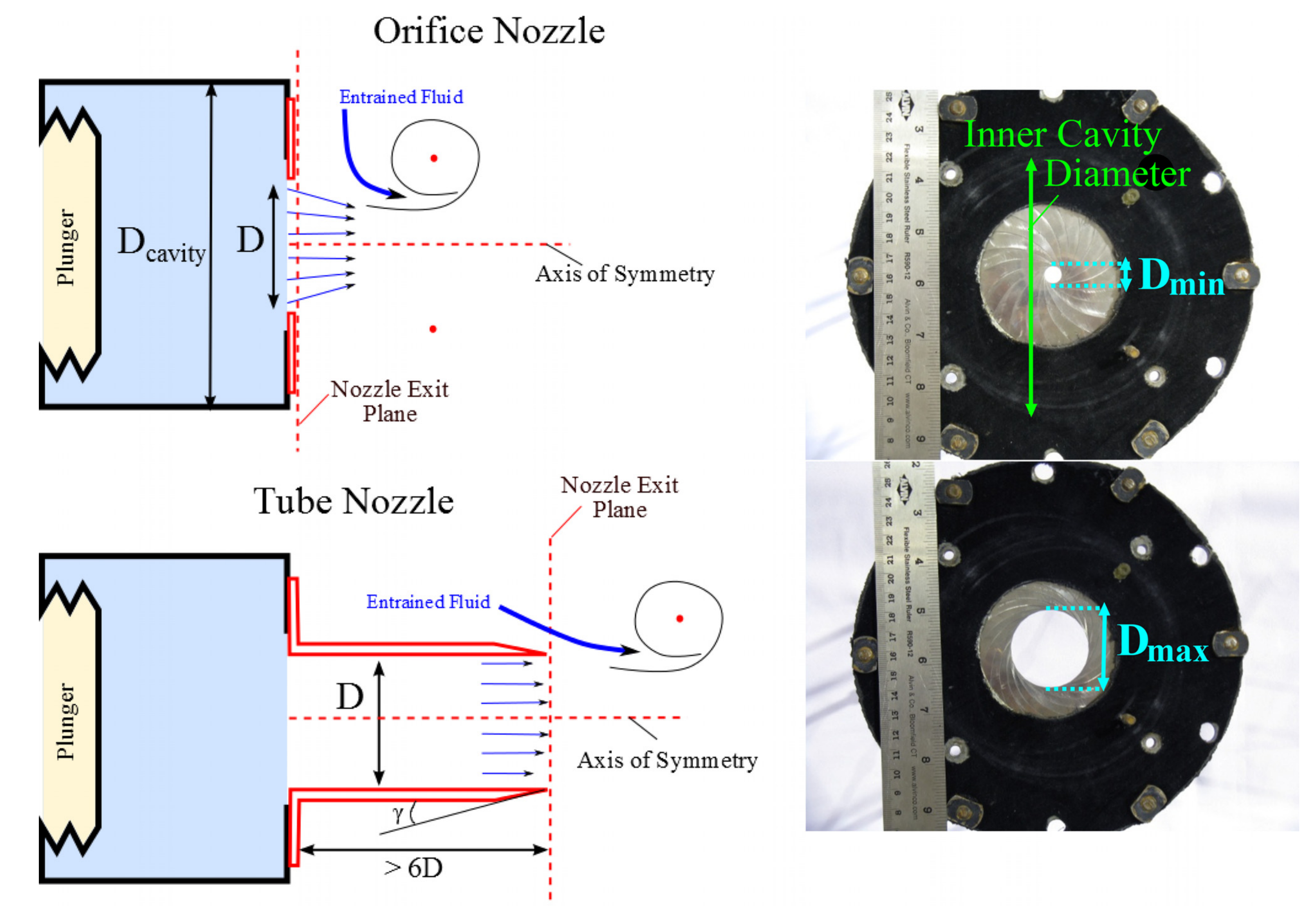

(a) Static Nozzle Configurations (b) Variable Diameter Nozzle

FIG. 3. Conceptual diagram of the layout of different nozzles used to generate various jet flows for this experimentation (a) and the variable diameter nozzle shown at the limits of diameter actuation (b).

GAM 1000B) expanded through a cylindrical lens within the tank. The illuminated cross section of the flow is recorded using a high speed digital camera. The camera used is a monochrome Phantom v210.

The experimental trials examined in this investigation are summarized in Table I. Many of the jet flows examined in this study have a nearly impulsive velocity program. This means that the piston velocity of the jet rapidly accelerates at the onset of flow, and then maintains a nearly constant piston velocity for the remainder of pulsation. The jets with constant piston velocity and nozzle diameter (cases 1 and 2 in Table I) provide a good baseline for validating the pinch-off criteria for the different nozzle configurations; however, a complete validation of the pinch-off criteria requires testing of jets flow with both an accelerating piston velocity (cases 3–5) as well, since the accelerating velocity program has been predicted to increase formation number. For these trials both parallel and converging jets were created with linearly accelerating piston velocity and static nozzle radius.

The actual piston velocity programs of cases 1–5 are presented in Fig. 5. These velocity programs were determined from the recorded motor encoder data.

C. DPIV analysis description

The high speed video of the jet flow is analyzed using a commercial software, with DPIV algorithms similar to those described in Refs. 40 and 41 to determine a velocity field $\vec{u} = [v, 0, u]^T$ in the illuminated cross section of the jet flow. Frames (1280×800 pixel resolution), were divided into 36×36 pixel interrogation windows (with 50% overlap). Depending on exact nozzle diameter and optical zoom, the total DPIV velocity field domain ranged from 3.83×6.12 diameters to 5.22×8.35 diameters, with the long dimension aligned with the axis of symmetry, resulting in relative resolutions in the range 10–12 grid points per nozzle diameter. Strict care was taken to ensure that the laser sheet bisected the flow through the jet axis of symmetry, so that the filmed jet flow corresponds to the axisymmetric flow. An example of the velocity and vorticity fields determined through this process is shown in Fig. 6.

Again, the flow is assumed to be axisymmetric with no swirl. Therefore, the total circulation, hydrodynamic impulse, and kinetic energy of the control volume can be calculated from the vorticity and velocity fields[42,43]

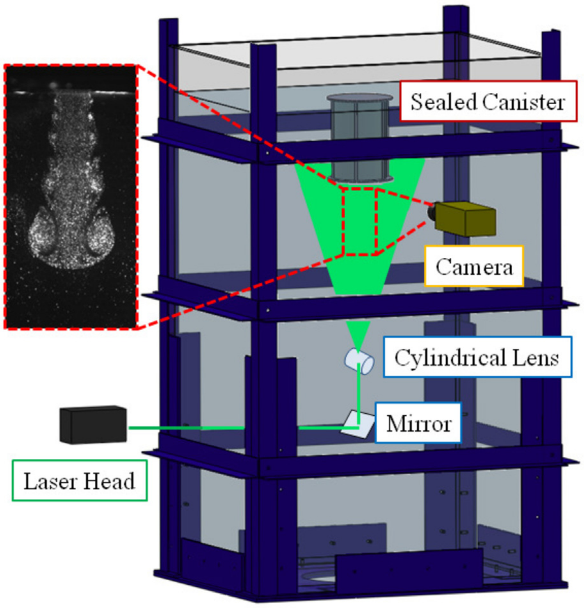

FIG. 4. Arrangement of the flow visualization setup.

$$\Gamma = \int_0^\infty \int_0^\infty \omega \, drdx,$$
$$I = \rho\pi \int_0^\infty \int_0^\infty \omega r^2 drdx, \tag{16}$$
$$E = \rho\pi \int_0^\infty \int_0^\infty (u^2 + v^2) r \, drdx.$$

The axisymmetric formulation implies that the velocity/vorticity field is known for a single half plane extending from the axis of symmetry. The DPIV analysis determines the velocity field for the entire plane which gives two axisymmetric sections π rad out of phase. In general, quantities of interest will be calculated for both half planes given by DPIV analysis and averaged to give a more accurate value. Variation between the vorticity distributions in the two half-planes is quantified with respect to the existence of azimuthal waves in the Appendix, as it is related to a variable diameter nozzle. Those variations were seen to be largely negligible.

The boundary of the vortex ring core, δ, is determined from the vorticity field as an isovorticity contour at some small threshold value $\omega_\epsilon = 4 - 6\,\text{s}^{-1}$, which is above the background noise level (this can be seen as the lowest level isovorticity contour in Fig. 6). It should be noted that the isovorticity contour corresponding to the threshold, ω_ϵ, often includes multiple rings in the trailing wake. Therefore, the leading vortex ring core boundary is determined as the closed isovorticity contour enclosing the peak vorticity. Defining the core area, A_c, as the region encompassed by the core boundary, δ, the circulation, impulse, and energy of the leading vortex ring can be determined from the same integrands as the total quantities with a closed boundary of integration

$$\Gamma_c = \int_{A_c} \omega \, drdx,$$
$$I_c = \rho\pi \int_{A_c} \omega r^2 \, drdx, \tag{17}$$
$$E_c = \rho\pi \int_{A_c} (u^2 + v^2) r \, drdx.$$

The center of vorticity of the vortex ring, used to determine translational velocity for the SG velocity criterion, is not necessarily at the same location as the peak vorticity value. The definition of the center of vorticity is given in Refs. 37 and 44 in terms of vorticity integral quantities. Restricting the integrals to the vortex core area, A_c, allows the vortex centroid to be determined

$$l^2 = \frac{\int_{A_c} \omega_\phi r^2 \, drdx}{\int_{A_c} \omega_\phi \, drdx}, \quad x_c = \frac{\int_{A_c} \omega_\phi r^2 x \, drdx}{\int_{A_c} \omega_\phi r^2 \, drdx}. \tag{18}$$

Now the circulation, impulse, and energy of experimentally generated jet flows and characteristics of the leading vortex ring can be determined from DPIV data, which allows validation of the different pinch-off criteria.

IV. RESULTS

A. Validating selection of characteristic induced and feeding velocities

The vortex ring pinch-off criterion/prediction analysis of Sec. II relies on the approximation of the velocity at the origin of a translating vortex ring. This section addresses the accuracy of this approximation.

This manuscript recommends using the centerline velocity of the vortex ring, $u_* = u(0, x_c)$, as the characteristic vortex velocity to define a kinematic pinch-off criterion. The methodology asserted that this induced velocity could be calculated as the centerline velocity of an equivalent filament vortex ring, identical circulation and impulse

TABLE I. Summary of experimental trials.

Case	Description	u_p (cm/s)	Nozzle type	Nozzle radius (cm)	Re
1	Constant u_p, R	7.5	Tube	0.91	7879
2	Constant u_p, R	7.4	Orifice	0.93	10 491
3	Accelerating jet	$(5 \rightarrow 14.7)$	Tube	0.91	11 096
4	Accelerating jet	$(2.1 \rightarrow 8.2)$	Orifice	0.98	49 771
5	Accelerating jet	$(4 \rightarrow 40)$	Tube	0.91	3266

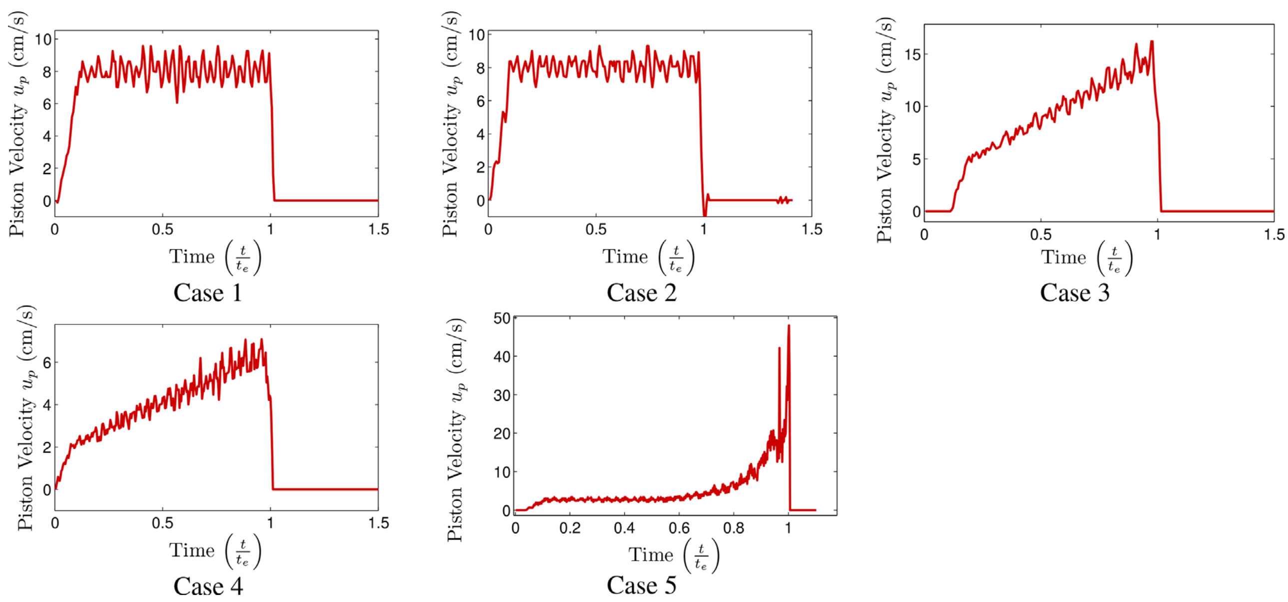

FIG. 5. Piston velocity programs for several trials, summarized as cases 1–5 in Table I.

(12). Here we look at the validity of that assumption. Figure 7 shows the actual centerline velocity of vortex rings created from both converging and parallel jet flows (cases 1 and 2), and the approximated centerline velocity calculated from (12) using values for ring circulation and impulse determined from DPIV data (17). For both cases, the stroke ratio is large $L/D \approx 7$, which corresponds to a more energetic pinch-off process resulting in larger oscillations in the translational velocity of the vortex ring.

There are three crucial stages associated with the entire starting jet pulsation. First, the jet flow is initiated and the shear layer begins to roll into the leading vortex ring. Next, the vortex ring becomes saturated and the feeding shear layer becomes destabilized. As was mentioned previously, vortex ring pinch-off is not an instantaneous process, and during this stage the vortex ring is dynamically evolving into a stable structure but cannot be discerned from the destabilized shear flow. Finally, the leading vortex ring settles on a stable configuration and propagates downstream.

To help with the induced velocity validation during the middle transformative stage, we also calculate the ring circulation and impulse assuming a more heuristic core boundary. The alternative core boundary is approximated as a circle centered on the peak in vorticity with core radius set to 0.9 times the toroidal radius of the peak vorticity filament. The value 0.9 corresponds to a maximum mean core radius observed in the trials. Using this approximate core boundary, we can calculate the ring circulation and impulse from (17) and induced velocity from (12) as was done for the isovorticity core boundary. It should be noted that the definitions of core boundary here are used exclusively to validate the induced velocity approximation, and have

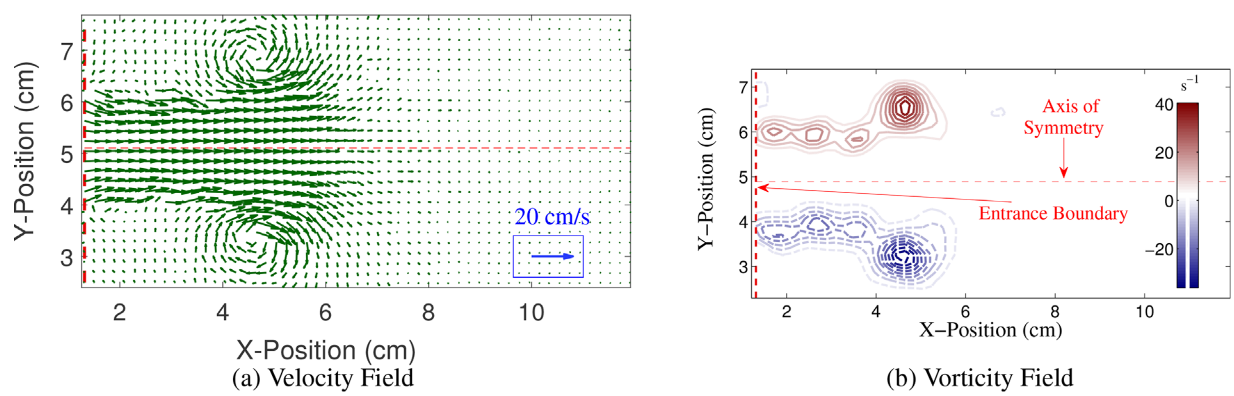

FIG. 6. Sample image of the velocity field (a) and vorticity field (b) determined from the DPIV analysis. The axis of symmetry is shown by the dashed red line running horizontal through the center and the vertical dashed line marks the nozzle exit plane. This sample flow field was generated by a jet ejected from an orifice nozzle with a nozzle radius of 0.93 cm and a piston velocity of $\approx$7 cm s^{-1}. This corresponds to experimental case 2, as summarized later in Table I. This figure has been reproduced with permission from M. Krieg and K. Mohseni, J. Fluid Mech. **719**, 488 (2013). Copyright 2013 Cambridge University Press.

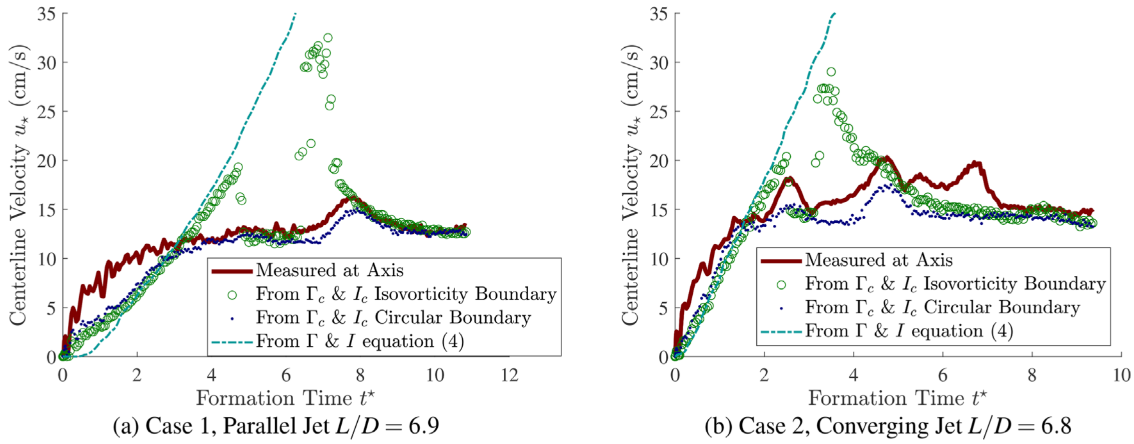

FIG. 7. Centerline velocity of the vortex ring, u_*, vs formation time t^*. Actual values calculated from PIV velocity data along axis of symmetry and predicted values calculated from Eq. (12) using measured values of Γ_c and I_c. The centerline velocity of a ring created from a parallel jet is shown in (a) and values for a ring created from a converging jet are shown in (b). The formation numbers measured for each of these runs are 4.28 (a) and 2.18 (b), respectively.

no impact on the use of the new pinch-off velocity criterion as a predictive tool. In order to predict the formation number for a given set of operational parameters, the entire jet is assumed to be in the vortex ring to calculate induced velocity and pinch-off is predicted when this velocity surpasses the maximum feeding velocity. As such, we have also included the induced velocity if the ring impulse and circulation are calculated from (4) to predict induced velocity. It should be noted that results on measured formation number in Secs. IV B 1 and IV B 2 require that core boundary be identified to calculate ring circulation. In those sections the ring circulation is only measured after it has settled on a stable configuration, so there is no ambiguity in the separation between primary ring and trailing jet, and the isovorticity contour at level ω_ϵ is used to define the core boundary.

During the final stage when the vortex rings are in a stable configuration, the centerline velocity calculated by (12) is nearly identical to the actual induced velocity, for both definitions of core boundary, despite the significant core size of the final vortex rings. This confirms that the thin core approximation does not significantly reduce the accuracy of calculating induced velocity at the origin. During the first phase, the calculated centerline velocity generally under-predicts the actual velocity. This is due to the fact that the induced velocity is lower than the feeding velocity while the ring grows, so the centerline velocity is inflated by the feeding jet flow. During the dynamic pinch-off phase, after the shear flow has become destabilized but before the ring has settled on a final configuration, the leading ring cannot be identified separately from the trailing shear flow, but it is no longer receiving additional energy/circulation from that trailing flow. Since the boundary identified by the threshold vorticity isocontour, ω_ϵ, includes a portion of the trailing shear flow that no longer influences the leading ring, Eq. (12) predicts a higher centerline velocity than is seen in the evolving ring. Alternatively, if the core boundary is just assumed to be a circle of appropriate mean core radius around the peak in vorticity, then the induced centerline velocity again becomes a reasonable approximation of the actual centerline velocity, although slightly under-predicted, again confirming the accuracy of the induced velocity approximation throughout the jetting process. It should be noted that the u_* model predicts an accurate centerline velocity when the shear layer first begins to become destabilized, and the model goes from under-predicting to over-predicting at the exact formation time associated with pinch-off, as will be seen in Sec. IV B 1.

The velocity profile along the axis of symmetry is plotted in Fig. 8 at several characteristic times for experimental case 2 as a representative example. It can be seen here that in the early formation phase ($t^* = 1.37$) the axial velocity increases smoothly reaching a peak at the axial location of the leading vortex ring, and no distinction is seen between the ring and feeding shear flow. As mentioned before, the actual ring separation from the feeding flow is not an instant action, but a longer dynamic process, thus it is impossible to identify flow of the leading vortex ring as independent of the flow of the feeding jet until a formation time considerably later than the formation number. At $t^* = 2.37$ just after the induced velocity surpasses the limit of a fully developed shear layer, $u_* \geq 2u_p$ the velocity profile along the axis of symmetry forms a deficit behind the forming vortex ring as the trailing shear layer begins to destabilize. The full velocity field of the jet flow at this instant is shown in Fig. 9. The axial component of velocity is shown by a contour map and the full axisymmetric velocity is depicted by a vector field laid on top. The location of the center of the leading vortex ring is marked by a solid dot and the isovorticity contour at level ω_ϵ, denoting the boundary of the combined ring and shear layer, is depicted by the solid red line. It can be seen in this figure that the velocity induced by the vortex remains relatively constant moving radially outward from the central axis, including the region where the shear layer connects to the vortex ring, validating the use of u_* as the characteristic induced velocity. Finally, as shown in Fig. 8, as the vortex ring begins to settle on a stable configuration, two distinct peaks can be seen in the velocity profile along the axis corresponding to the separated vortex ring and trailing shear flow.

B. Validation of pinch-off criteria and formation number of jet flows

Now that the velocity approximations have been validated, we will examine the exact formation number of different starting jet flows, and the validity of the different kinematic pinch-off criteria. Starting

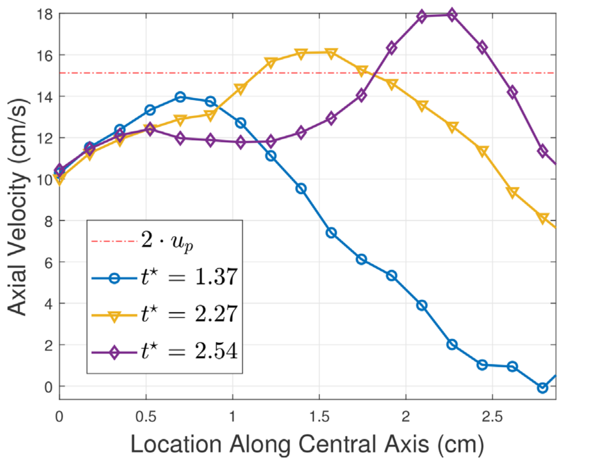

FIG. 8. Axial velocity along the central axis at multiple characteristic times during the vortex ring formation process for experimental case 2 (the formation number measured for this case was 2.18).

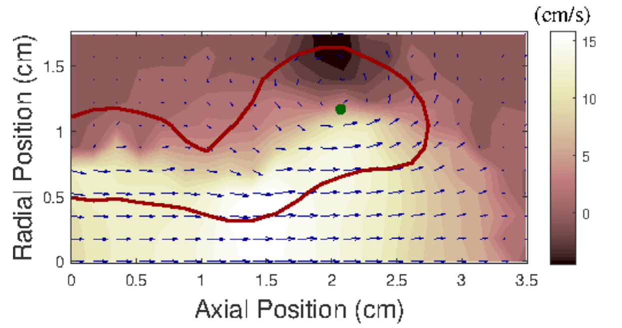

FIG. 9. Plot of the velocity field near the axis of symmetry for experimental case 2 at formation time $t^* = 2.27$. The vector field shows the full 2D velocity, while the magnitude of the axial component of velocity is shown with a contour plot in the background. The solid red line shows an isovorticity contour equal to ω_ϵ denoting the combined boundary of the vortex ring and feeding shear flow. The center of vorticity is marked by a solid green dot.

with the most simple flow having constant piston velocity, u_p, and static nozzle ($R =$ constant). A converging radial velocity significantly decreases the jet formation number, and this is accurately captured by the centerline velocity criterion used in this paper. After analyzing these simple constant velocity cases with different nozzle geometries, an accelerating piston velocity program is investigated exhibiting an increased formation number over the constant piston velocity jet with the same nozzle configuration. The new pinch-off criterion is observed to be valid for the conditions tested here.

1. Constant u_p, effect of converging radial velocity on formation number

From a qualitative standpoint, the larger induced and translational velocity of the vortex ring formed by the converging jet[45] should cause a decrease in formation number if the kinematic pinch-off criteria truly corresponds to the vortex ring separation mechanism.

The circulation for a parallel starting jet is plotted with respect to formation time in Fig. 10(a) (case 1) next to the circulation for a converging starting jet in Fig. 10(b) (case 2). The vortex core boundary was identified as described in Sec. III C. The circulation integrated over this region, after the primary vortex ring had settled, is also shown for both jet flows. Some time after the jet flow has been terminated the total circulation drops accounting for vorticity cancelation at the axis of symmetry. This decay is typical of thick vortex rings and has been reported in Ref. 18, and also the unstable shear layer is compressed toward the axis of symmetry just before separation, as was described in Sec. II (Fig. 2), adding to the vorticity cancelation. In addition to the cancelation of vorticity, the large trailing wake becomes unstable with time which can result in bifurcation/blooming of vortex rings in the wake, making the flow asymmetric about the centerline and driving the vortex rings in the wake out of the illuminated cross section. See Ref. 46 for a description of blooming jets.

Figure 10 demonstrates that vortex rings formed from converging starting jets pinch-off at a significantly lower formation time. It can be seen that the formation number for the parallel jet is ≈ 4 as would be expected, but the formation number for the converging jet drops to ≈ 2.3, which is very close to the formation number predicted by the centerline velocity pinch-off criterion of this paper, 2.1, under the assumption of constant piston velocity (15). Figure 11 shows the induced velocity on the centerline, u_*, defined by (12), as well as the feeding velocity, $2u_p$, for the two jet flows represented in Fig. 10 (cases 1 and 2). It can be seen here that the induced velocity surpasses the feeding velocity almost exactly at the formation number for both types of jet flows, affirming the use of the centerline kinematic criterion for predicting pinch-off in both parallel and non-parallel starting jets with constant velocity and radius driving programs.

Figure 12 shows the vortex ring translational velocity, U_{tr} (determined from the motion of the vortex centroid) as a function of formation time as well as the adjusted jet velocity in accordance with the SG velocity criterion. To determine the adjusted jet velocity, the vortex ring radius was calculated from DPIV data according to Eq. (18). This criterion predicts pinch-off at a later formation time than observed, mostly because the axial velocity at the jet/ring interface is substantially larger than the propagation velocity. Furthermore, the large fluctuations in both translational velocity and toroidal radius (used to calculate the adjusted jet velocity) result in some ambiguity of predicted formation number for the converging jet. This is because as the vortex translational velocity approaches the adjusted jet velocity, it drops briefly before increasing again and does not distinctly surpass the adjusted jet velocity until well after pinch-off has occurred. The ambiguity is more noticeable for the converging jet, as shown in Fig. 12(b).

It is not exactly clear that the shift in formation number associated with a converging radial velocity is due to a change in the final vortex ring configuration. The drop in formation number seen in starting jet simulations with fully developed pipe flow at the entrance boundary (see Ref. 15) is closely related to the definition of formation time. As was pointed out by Rosenfeld *et al.*, the rate of circulation flux across the entrance plane for parallel starting flows is exactly proportional to the centerline velocity, $d\Gamma/dt = \frac{1}{2}u_0^2$, independent of the jet axial velocity profile. However, the formation time is scaled by the piston velocity, which is much less than the centerline velocity for parabolic jet velocity profiles, meaning that flows with a parabolic velocity

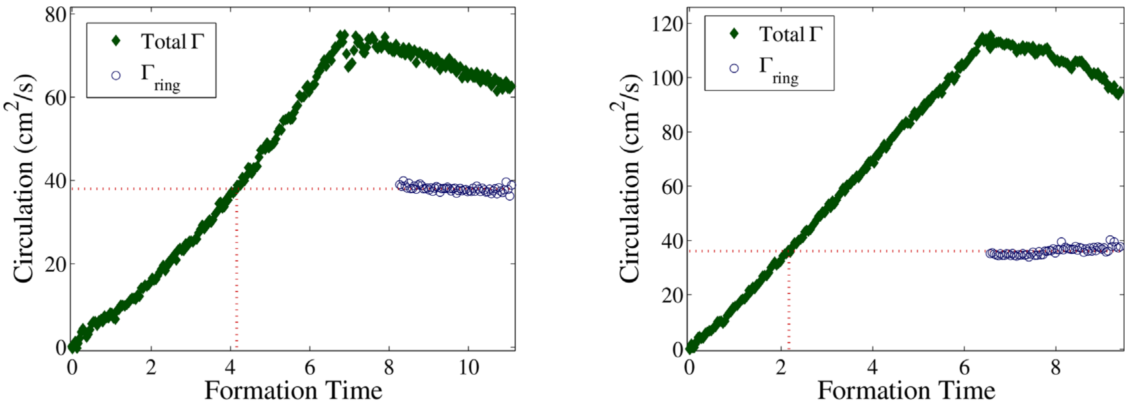

(a) Case 1, Parallel Jet, $L/D = 6.9$ (b) Case 2, Converging Jet, $L/D = 6.8$

FIG. 10. Circulation vs formation time of both the entire jet and the leading vortex ring for typical parallel and non-parallel starting jets. Experimental case 1 is shown in (a) and case 2 is shown in (b).

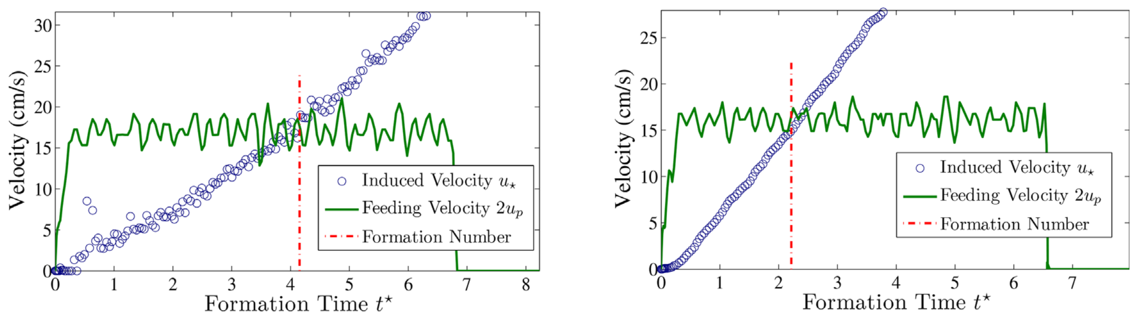

(a) Case 1, Parallel Jet (b) Case 2, Converging Jet

FIG. 11. Induced and feeding velocity vs formation time for jets created with tube and orifice nozzles. Formation number for these cases, as determined from final circulation values, is also shown. Experimental case 1 is shown in (a) and case 2 is shown in (b).

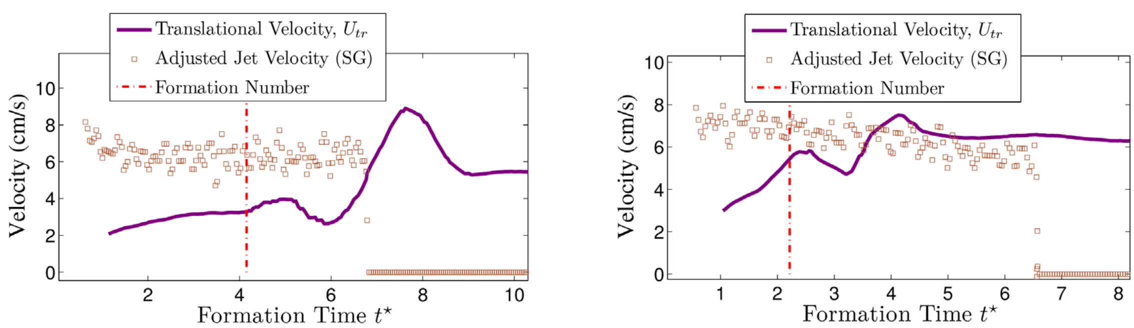

(a) Case 1, Parallel Jet (b) Case 2, Converging Jet

FIG. 12. Propagation and adjusted jet velocity vs formation time for jets created with tube and orifice nozzles. Experimental case 1 is shown in (a) and case 2 is shown in (b).

profile will produce a higher vorticity flux for the same volume flux compared to flows with a uniform velocity profile. Similarly, converging starting jets generate a significantly larger vorticity flux than the parallel starting jet with the same piston velocity, refer to Ref. 16 for the exact increase in circulation. As would be expected, these flows have a formation number, much lower than the trend seen in Ref. 1.

In order to further analyze any change in the final vortex ring configuration from these two cases, we calculate the non-dimensional

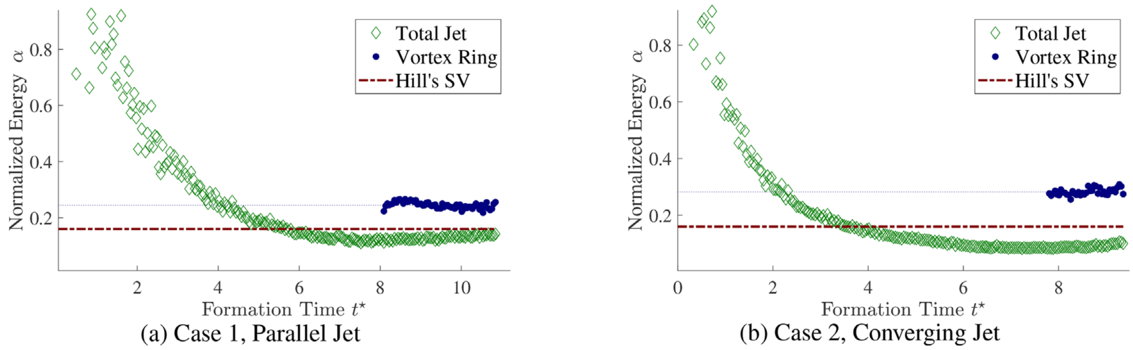

FIG. 13. Non-dimensional energy, α, vs formation time of the total jet and the leading vortex ring for parallel (a) and non-parallel (b) jet flows. Also shown is the theoretical minimum stable non-dimensional energy corresponding to Hill's spherical vortex ring (maximum thickness). The formation numbers measured for each of these runs are 4.28 (a) and 2.18 (b), respectively.

energy, α, of both the total jet flow and the separated vortex ring. Recall that non-dimensional energy is large for thin cored vortex rings and decreases as the vortex ring becomes fuller, achieving a theoretical minimum of 0.16 for Hill's spherical vortex. The non-dimensional energy of vortex rings generated from parallel and converging starting jets (cases 1 and 2) is shown in Fig. 13. The energy of the parallel jet vortex ring settles to about $\alpha = 0.242$. This is slightly lower than the values found in Ref. 1 for parallel jets, which had a non-dimensional energy on the order of $\alpha = 0.33$. The energy of the converging jet vortex ring is slightly larger $\alpha = 0.285$, corresponding to a "thinner" vortex ring. This indicates that the centerline velocity criterion accurately predicts pinch-off without requiring a specified final ring configuration.

So far the dynamics of vortex ring pinch-off have been discussed in terms of representative examples for each jetting case. The pinch-off process is a dynamic reorganization of vorticity distribution which varies from trial to trial, so we plot circulation and velocity graphs for individual trials. However, for each experimental case, we have conducted multiple trials to examine the consistency of results. Table II is provided to summarize the formation number, and final non-dimensional energy of all cases studied here. The table also lists the number of trials performed for each case and the standard deviation of the measured parameters. While different trials for each case maintained a given nozzle geometry and velocity program type, for many cases the value of the piston velocity was allowed to vary to observe the consistency of final ring configuration over a range of jet velocities. The table also lists the jet radial velocity parameters k_1^* and k_2^*, which are averaged over the jetting duration to demonstrate that these values are largely dependent on nozzle geometry rather than other jetting parameters.

As can be seen in Table II, the mean formation number measured for case 1 was 4.16 with a standard deviation of 0.1. The velocity criterion proposed here predicted a formation number as low as 3.95 in the worst performing trial which is within two standard deviations of the average. The SG velocity criterion predicted formation number 6.97 which is 28 standard deviations away from the average. Similarly, for case 2, the centerline velocity criterion predicted formation number as high as 2.7 which is within two standard deviations for that case, and the SG criterion predicted a formation number as high as 3.69 which is more than five standard deviations from the average.

Next we extend our analysis to include more complicated jetting programs, more specifically an accelerating piston velocity program, while using static nozzles.

2. Accelerating piston velocity

It was hypothesized earlier in Sec. II that the formation number could be increased for a given vortex ring configuration by accelerating the jet flow to compensate for the quickly accelerating induced velocity; additionally simulations in Ref. 18 show that accelerating the jet flow is one of the two ways to change the jet formation number. To investigate this, the vortex generator was first driven with a linearly increasing piston velocity. Figure 14 shows the total jet circulation as well as the circulation of the primary vortex ring for both parallel and converging jets with the accelerating velocity programs depicted in

TABLE II. Summary of jet formation number for different driving conditions. The column *n* defined the number of trials run for each test case.

Case	Description	Nozzle type	n	u_p Range	k_1^*	k_2^*	τ	α
1	Constant u_p, R	Tube	4	6.5–10.7	0.04 ± 0.04	0.24 ± 0.13	4.16 ± 0.10	0.23 ± 0.02
2	Constant u_p, R	Orifice	4	4.6–10.8	-0.41 ± 0.05	1.07 ± 0.15	2.22 ± 0.28	0.33 ± 0.05
3	Accel jet (linear)	Tube	3	$(5 \rightarrow 14.7)$	0.00 ± 0.03	0.30 ± 0.13	4.21 ± 0.22	0.24 ± 0.03
4	Accel jet (linear)	Orifice	2	$(2.1 \rightarrow 8.2)$	-0.13 ± 0.18	0.88 ± 0.03	3.66 ± 0.29	0.22 ± 0.01
5	Accel jet (match)	Tube	1	$(4 \rightarrow 40)$	0.02	0.10	8.19	0.20

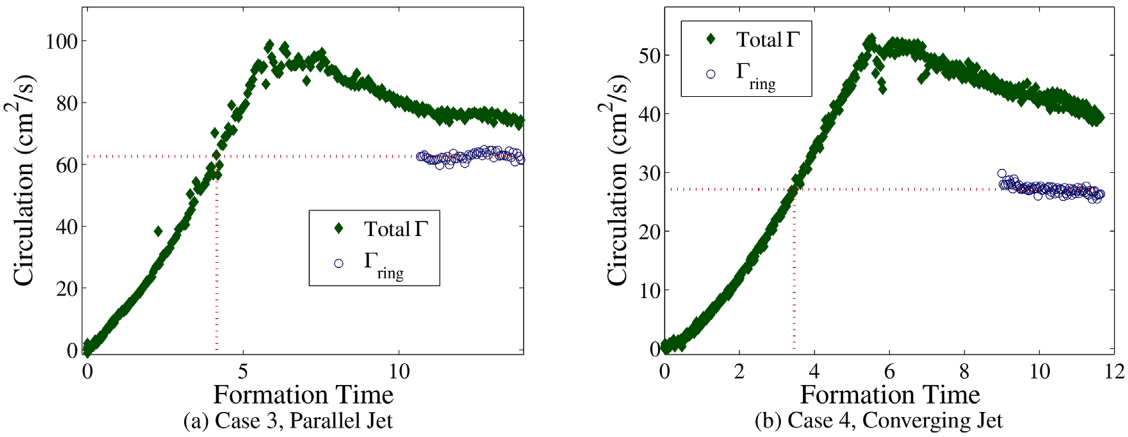

FIG. 14. Circulation vs formation time for both parallel (a) and converging jets (b) with large stroke ratios and accelerating piston velocities. Exact velocity programs are given in Fig. 5.

Fig. 5 (cases 3 and 4). It can be seen that the formation number of the converging jet with linearly accelerating velocity program is 3.8, which is a drastic increase over the formation number of the jet expelled through the same nozzle with a constant piston velocity which has a formation number $\tau \approx 2.3$. However, the linearly accelerating velocity program does not significantly increase the formation number of the parallel jet which is 4.2 for this case. This indicates that the linearly accelerating piston velocity program is still insufficient to compensate for the acceleration of the vortex ring itself. This is hardly surprising because velocity programs similar to the linear acceleration program were tested in the work of Gharib *et al.*[1] and the formation number remained in the universal bound $3.6 \leq t^*_{FN} \leq 4.2$.

But the question remains as to whether or not a more drastic piston velocity acceleration program can compensate for the accelerating vortex ring and increase the formation number beyond the maximum value of 4.2. To test this, we operated the vortex generator with a velocity program designed to match the predicted centerline velocity of the vortex ring as it grows (12), using the tube nozzle. The velocity program for this case is also shown in Fig. 5 (case 5) and can be observed to have a very drastic acceleration toward the end of pulsation. The total circulation and vortex ring circulation for this jet are shown in Fig. 15, demonstrating that the more drastic acceleration substantially increases the formation number of the jet to 8.2. It should be noted that this is also very close to the maximum formation number observed by Dabiri and Gharib[20] using a variable diameter nozzle, which is discussed in more detail in the Appendix.

Figure 16 shows that the centerline velocity criterion still coincides with the jet formation number even for jets with linearly accelerating piston velocity.

The non-dimensional energy of the vortex rings is shown in Figs. 17(a)–17(c), which shows that after pinch-off the vortex ring of the parallel linearly accelerating jet settles on a configuration with energy $\epsilon = 0.218$, the final energy of the converging linearly accelerating vortex ring is $\alpha = 0.227$, and the energy of the vortex ring generated with a matching velocity program is $\alpha = 0.198$. This means that jets with accelerating piston velocity are able to create significantly "thicker" vortex rings than jets expelled with a constant piston velocity. In fact the vortex ring created by an accelerating jet designed to match the ring velocity settles on a non-dimensional energy which nearly reaches the limit of Hill's spherical vortex corresponding to maximum thickness. It can also be seen in Fig. 17(c) that the feeding jet flow matches the ring velocity, as designed, for an extended period of the pulsation. The ring pinches off when the feeding jet can no longer match this velocity due to physical limitations.

V. DISCUSSION AND CONCLUSION

This study examined the critical point in vortex ring formation, known as pinch-off, where the ejected shear flow can no longer feed growth of the forming vortex ring in its current configuration, and it separates from the trailing shear flow. We suggest that this critical

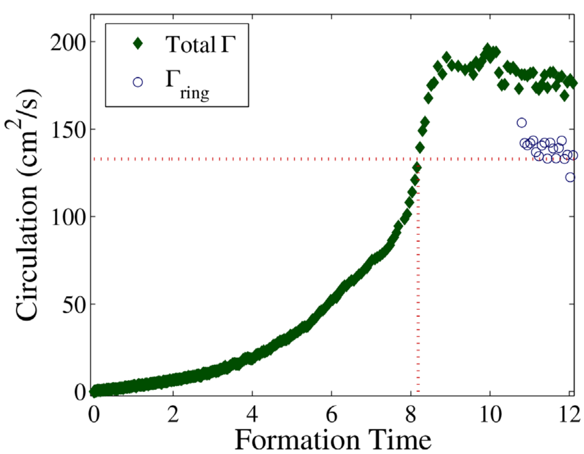

FIG. 15. Circulation vs formation time for a parallel jet expelled with a piston velocity program designed to match the vortex ring centerline velocity. The exact velocity profile is given in Fig. 5 (case 5).

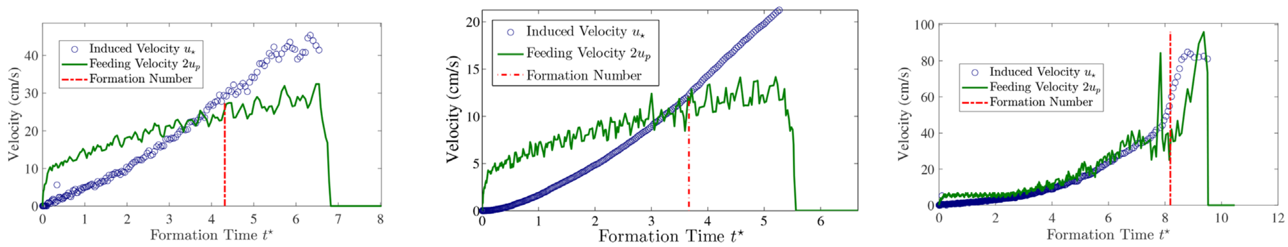

(a) Case 3, Parallel Jet (b) Case 4, Converging Jet (c) Case 5, Parallel Jet Matching Program

FIG. 16. Feeding and induced velocity of the accelerating jet vs formation time. Experimental case 3 is shown in (a), case 4 is shown in (b), and case 5 is shown in (c).

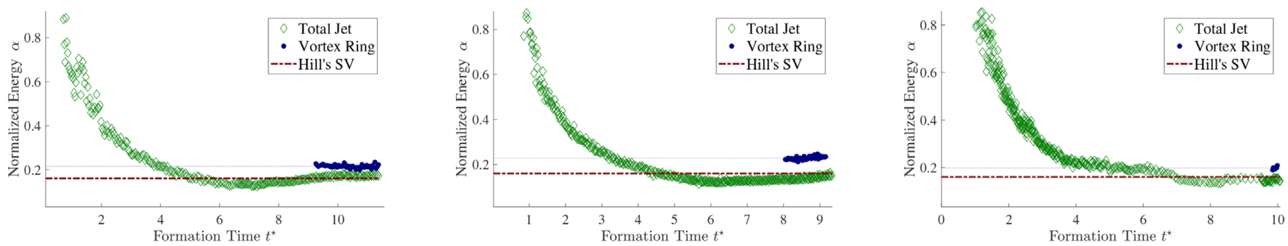

(a) Case 3, Parallel Jet (b) Case 4, Converging Jet (c) Case 5, Parallel Jet Matching Program

FIG. 17. Non-dimensional energy, α, vs formation time of the total jet and the leading vortex ring for parallel (a) and (c) and non-parallel (b) jet flows. Also shown is the theoretical minimum stable non-dimensional energy corresponding to Hill's spherical vortex ring (maximum thickness). The formation numbers measured for each of these cases are 4.43 (a), 3.46 (b), and 8.19 (c), respectively.

configuration can be identified as the moment when the velocity along the axis of symmetry induced by the vortex ring surpasses the maximum available feeding velocity at the axis of symmetry. Unlike the velocity criterion suggested by Shusster and Gharib, this velocity criterion considers both the feeding and vortex ring velocities to be nonuniform and identifies a specific interface location, which is observed to correlate better with pinch-off in a wide variety of experimentally generated jet flows.

This criterion for vortex ring pinch-off can also be used as an analysis tool to help understand starting jet flows not investigated here. For example, pinch-off has not been observed for very large stroke ratio starting jets ejected from rectangular slits,[34] which can be understood in terms of the characteristic induced and feeding velocities. If two jets are ejected with a similar piston velocity, one through a long slit with some thickness and one through a circular nozzle with diameter equal to the slit thickness, then the two jets will have a similar (though not equivalent) centerline velocity. Therefore, the rate of circulation generated in the two jets is on the same order of magnitude. However, due to the large length of the slit it has a much larger area, and the rate of impulse added to the jet is significantly higher. By Eq. (12) this will result in a significantly lower velocity induced by the forming vortex ring, thus allowing the shear flow to continue feeding the growth of the vortex core, or in other words, the asymmetry of the rectangular orifice allows the jet flow to achieve a much higher feeding velocity relative to the vortex induced velocity, helping us to explain why pinch-off has not been observed in these jet flows.

Using different nozzles, both parallel and converging starting jets were examined. It is found that converging starting jets had a substantially lower formation number because of the increased rate of circulation created in the converging jet. Ejecting the jet with an accelerating piston velocity program increased the formation number of both types of jets. The converging jet formation number increased from $\tau \approx 2$ to $\tau \approx 4$ when the velocity program was changed from a nearly impulsive program to a linearly accelerating program and the parallel jet formation number increased from $\tau = 4$ to $\tau = 8$ for a more drastically accelerating velocity program. For all cases, the new centerline velocity criterion coincided very well with vortex ring pinch-off.

ACKNOWLEDGMENTS

This work is supported by a grant from the Office of Naval Research.

APPENDIX: FORMATION TIME AND FORMATION NUMBER FOR VARIABLE DIAMETER NOZZLES

1. Formation time

The definition of formation time becomes ambiguous for jet flows expelled through variable diameter nozzles, and we need to define a characteristic scaling for the case of dynamic nozzles. Dabiri and Gharib[20] suggest

$$t^*_{\mathrm{DG}} = \int_0^t \frac{u_p}{D}\, d\tilde{t}, \tag{A1}$$

as a new definition for the formation time, which seems a logical choice but does not necessarily incorporate the dynamics of the problem. We suggest an alternative definition

$$t^*_{\mathrm{RMS}} = \frac{\int_0^t u_p\, d\tilde{t}}{2R_{\mathrm{RMS}}}, \tag{A2}$$

where R_{RMS} is the root mean square of the nozzle radius, $R_{\mathrm{RMS}} = [1/t \int_0^t R^2\, d\tau]^{1/2}$. Both definitions reduce to the original definition for static nozzles. However, we show here that Eq. (A2) maintains and inverse proportionality of the formation time with the ring non-dimensional energy, α. That being said, for jet flows with variable diameter nozzle in this study, the nozzle diameter program $R(t)$ is a linear function of time, so the two definitions will provide a roughly equivalent formation time.

Ideally a universal formation number, τ, corresponds to a universal vortex ring configuration (or thickness) for a variety of starting jet driving conditions. Although vortex ring thickness can be difficult to determine, the configuration can be uniquely identified by a parameter known as non-dimensional energy, given a particular vorticity distribution. The non-dimensional energy of the jet is defined as $\alpha = E_c/(I_c^{1/2}\Gamma_c^{3/2})$, as was done in Ref. 1. It can be shown that the formation time is in fact inversely proportional to the dimensionless energy of the jet if the piston velocity and nozzle radius programs are held constant.[14] If we assume that the axial velocity profile is constant and the radial velocity profile is linear, then the total circulation, impulse, and energy of the jet can be calculated from Eqs. (4) multiplied by the total pulsation time, t_e. Inserting these into the definition of, α, and rearranging terms results in the relationship

$$t^* = \frac{u_p t_e}{D} = \frac{C_\alpha}{\alpha}, \qquad C_\alpha = \sqrt{\frac{\pi}{2}} \frac{2 + k_2^*}{\left[4 + k_2^* - k_1^{*2}\right]^{1/2}\left[1 + k_2^*\right]^{3/2}} = \sqrt{\frac{\pi}{2}}\Bigg|_{k_1^*=k_2^*=0}, \tag{A3}$$

meaning that in a very loose generalization a universal formation number corresponds to a minimum dimensionless energy, α, and a universal final vortex ring thickness. Again, holding the piston velocity constant but allowing the nozzle diameter to vary during pulsation, the circulation, impulse, and energy calculated from Eqs. (4) will be the same as before, except that the terms R^2 will be replaced with R^2_{RMS}. Plugging these values back into the definition of α results in

$$\frac{u_p t_e}{2R_{\mathrm{RMS}}} = \frac{C_\alpha}{\alpha}. \tag{A4}$$

Only the definition of formation time in (A2) preserves the relationship between formation time, t^*, and dimensionless energy, α, for variable diameter jets with constant piston velocity.

The formation time is equal to the stroke ratio, L/D, at the end of pulsation, for cylinder piston devices. The definition of stroke ratio is not obvious for other types of vortex generators since the stroke length of the fluid manipulator is not necessarily equal to the length of the fluid slug; therefore, we will define the stroke ratio as the formation time at the end of pulsation for all cases.

Another time scaling related to starting jet flows and vortex ring formation was presented in Ref. 18. In this study, the characteristic velocity and length scales used to normalize time are the translational velocity, U_{tr}, and toroidal radius, l, of the final vortex ring, respectively,

$$t^*_{\mathrm{VR}} = \frac{U_{tr}}{2l}\, t. \tag{A5}$$

Part of the difficulty in modeling the pinch-off process comes from the fact that pinch-off is a phenomenon which is dependent on both the state of the forming, unsteady vortex ring and the state of the feeding shear flow which is manipulated by the jet driving programs. The definitions of formation time summarized in Eqs. (1), (A1), and (A2) are all normalized by velocity and length scales associated with the jet driving parameters. The time scaling of (A5) is unique since it is scaled by the characteristics of the vortex ring. Unfortunately, this definition is less than optimal for experimental studies, because it requires exact knowledge of the final state of the vortex ring which might not be available in all studies.

2. Variable diameter nozzle

The variable diameter nozzle is very similar in shape to the orifice nozzle. The mechanism is similar to an iris diaphragm/shutter used in photography, where a set of interwoven leaves can be actuated to increase or decrease the central opening diameter. Although the opening is not a perfect circle, technically a regular 20 point polygon (corresponding to the 20 leaves), it will be approximated as a circular opening. The variable diameter nozzle is constructed out of thin stainless steel leaves, about 0.5 mm (0.02 in.) in thickness. The nozzle diameter ranges from 0.64 cm (0.25 in.) to 4.5 cm (1.75 in.), but can only be actuated about 30% of the range in a single pulsation. The mechanism is shown in Fig. 3 at the maximum and minimum achievable diameters.

The deviation from a perfect circle might possibly lead to an increase in azimuthal waves previously observed in and modeled for small core vortex rings,[47–49] and these waves are known to affect the stability of vortex rings, which could in turn affect the pinch-off dynamics. As was discussed previously, the measured velocity field extends through the axis of symmetry and contains a slice of the ring on either side of this axis. The existence of azimuthal waves traveling along the vortex ring would result in the toroidal radius of the ring being measured differently for one half than the other. To investigate the presence of these waves, we calculate a wave amplitude ratio, R_{WA}, which is the average difference in the measured value of toroidal radius over the entire run normalized by the average toroidal radius

$$R_{WA} = \frac{\frac{1}{T}\int_0^T l_1 - l_2\, dt}{\frac{1}{T}\int_0^T \frac{l_1 + l_2}{2}\, dt}, \tag{A6}$$

where l_1 is the toroidal radius measured in the plane on one side of the axis of symmetry, and l_2 is the radius measure in the plane on the other side. The wave amplitude ratio for case 1 (constant jet

TABLE III. Summary of experimental trials with dynamically changing nozzle diameter.

Case	Description	u_p (cm/s)	Nozzle type	Nozzle radius (cm)	*Re*
6	Increasing diameter	5.1	Orifice	(0.96 → 1.38)	3622
7	Decreasing diameter	3.3	Orifice	(1.23 → 0.84)	2056

velocity and tube nozzle) is $R_{WA} = 0.034$, indicating a low presence of azimuthal waves. This would be expected given the relative thickness of the vortex ring core. For a run with the same driving jet velocity program, and the variable diameter orifice nozzle set to a static diameter equal to that of the tube nozzle, the wave amplitude ratio was measured to be $R_{WA} = 0.027$, demonstrating that the shape of the nozzle does not increase the magnitude of azimuthal waves, and if anything, the more energetic ring is less prone to instability.

Table III summarizes additional test cases using the variable diameter nozzle. Case 6 has a linearly increasing nozzle diameter, and case 7 has a linearly decreasing nozzle diameter. For both of these cases, the volume flux of the vortex generator was compensated for the expanding or contracting nozzle radius in order to maintain a nearly constant piston velocity program. The measured velocity programs are shown in Fig. 18.

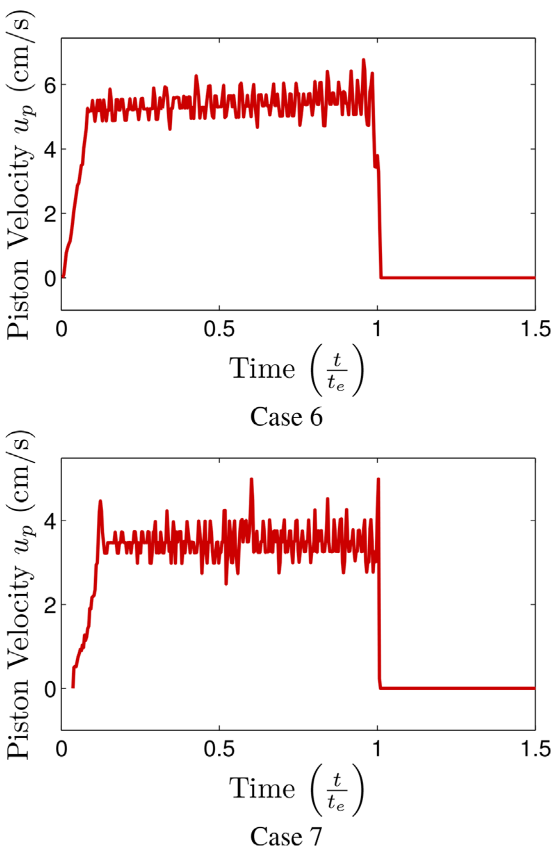

FIG. 18. Piston velocity programs for variable diameter test cases 6 and 7 in Table III.

3. Results from experimental cases with variable diameter nozzle and constant piston velocity

Here we would like to take a minute to note the nature of variable diameter nozzles. A jet flow discharging from a variable diameter nozzle will almost inherently contain some component of radial velocity. The most straightforward way to create a parallel jet flow with a variable diameter is to create a tube nozzle with the ability to expand uniformly along its length, which is well out of the range of our own manufacturing ability. Variable diameter nozzles which change conical shape dynamically pose an interesting problem since at some formation times they create a nearly parallel jet flow, and at other formation times they create a jet flow with significant radial velocity. This makes the effect of increasing/decreasing the radius of these types of nozzles difficult to determine independently since they are not functionally similar to any single type of static nozzle for comparison. The variable diameter nozzle of this investigation is an iris nozzle which is essentially a flat plate with an adjustable circular orifice in the center. This allows a direct comparison with static orifice type nozzles to determine the effect of increasing and decreasing nozzle radius, independent of any other changing factors.

The vortex generator was operated using the dynamic nozzle with both a linearly increasing and linearly decreasing nozzle radius program. The desired and actual nozzle radii for these tests are shown in Fig. 19, corresponding to cases 6 and 7 in Table I. Figure 19 also shows the toroidal radius of the leading vortex ring, demonstrating that an increasing radius nozzle will dynamically increase the vortex radius, but the most crucial factor controlling the vortex radius is the initial nozzle radius. For both cases the volume flux program, $\forall$ −(t), was designed to compensate for the variable nozzle diameter and maintain a constant piston velocity, despite the changing nozzle area.

Since the piston velocity is held constant and the nozzle radius program is nearly linear, the formation time defined by (A1) and (A2) are nearly identical, with some negligible variations due to an inability to guarantee a perfectly linear nozzle radius program. The total jet circulation and vortex ring circulation of the jets created with the nozzle radius programs depicted in Fig. 19 (cases 6 and 7) are plotted in Fig. 20 with respect to formation time as defined (A2). It can be seen in this figure that jets created with both increasing and decreasing nozzle radius have a formation number nearly identical to the constant diameter jet. This result is important because it demonstrates that changing the radius of the shear tube with a linear increasing/decreasing program during pulsation will not affect the formation number of the jet, at least not for the magnitudes tested here (variations of 30%–40% of the initial diameter). The numerical study performed by Mohseni *et al.* suggested that an increase in shear tube diameter with significantly larger magnitude will result in a decreased final non-dimensional energy, generally corresponding to an increased formation number. A direct

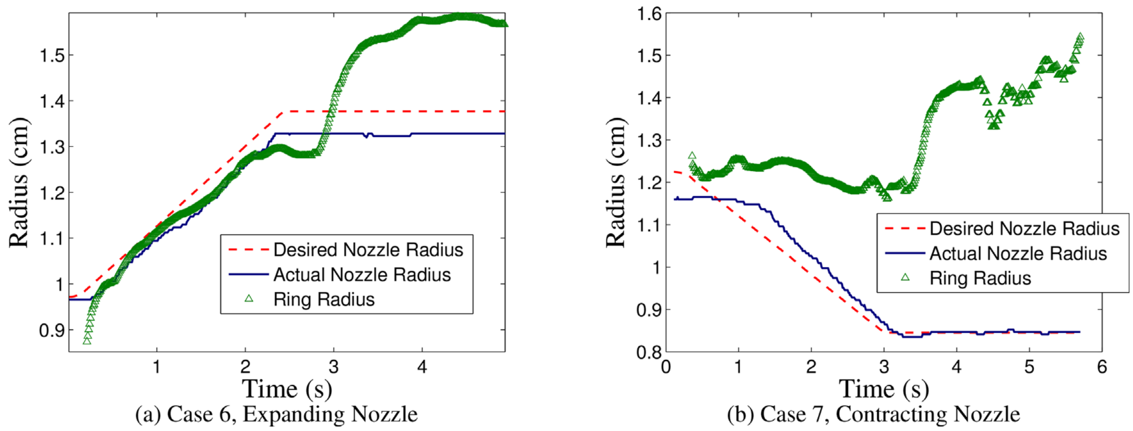

FIG. 19. The desired and actual nozzle radii are shown for increasing and decreasing radius programs. Also shown is the toroidal radius of the resulting vortex rings. Nozzle radius values for case 6 are plotted in (a) and case 7 in (b).

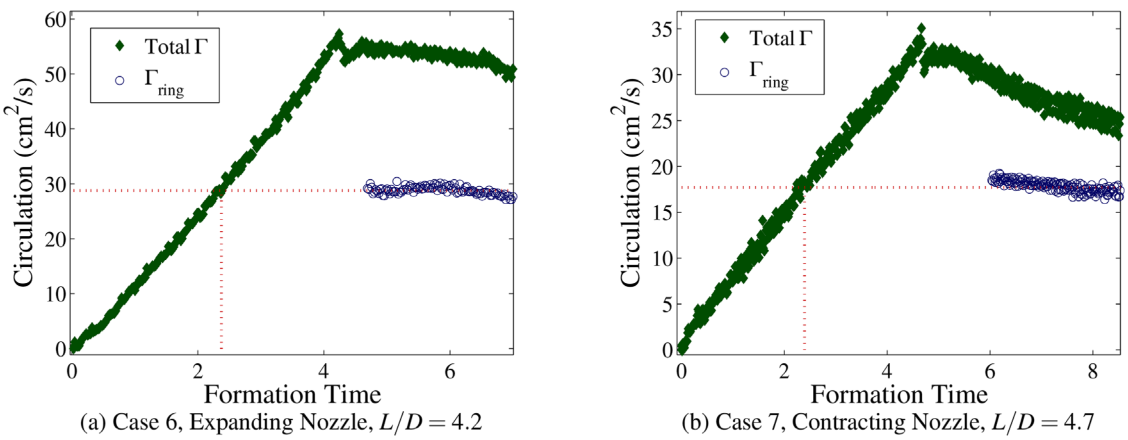

FIG. 20. Circulation vs formation time, as defined by (A2), for jets created with linearly increasing and decreasing nozzle radii. Experimental case 6 is shown in (a) and case 7 is shown in (b).

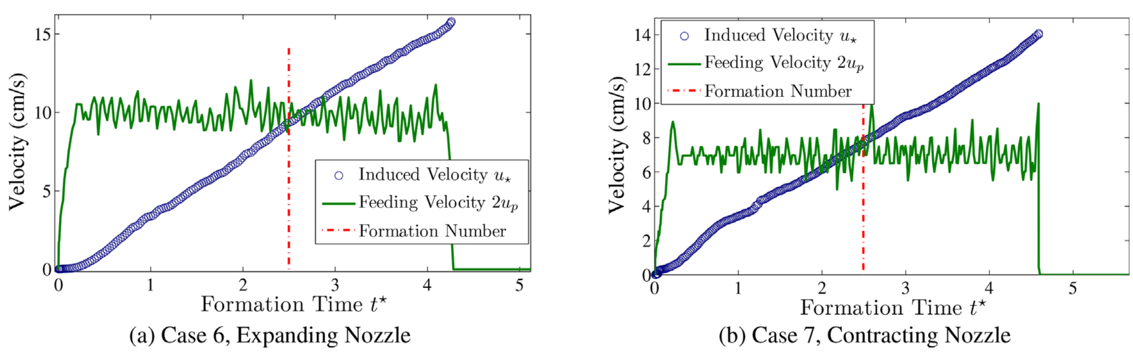

FIG. 21. Induced and feeding velocity vs formation time, as defined by (A2), for jets created with expanding and contracting nozzles. Experimental case 6 is shown in (a) and case 7 is shown in (b).

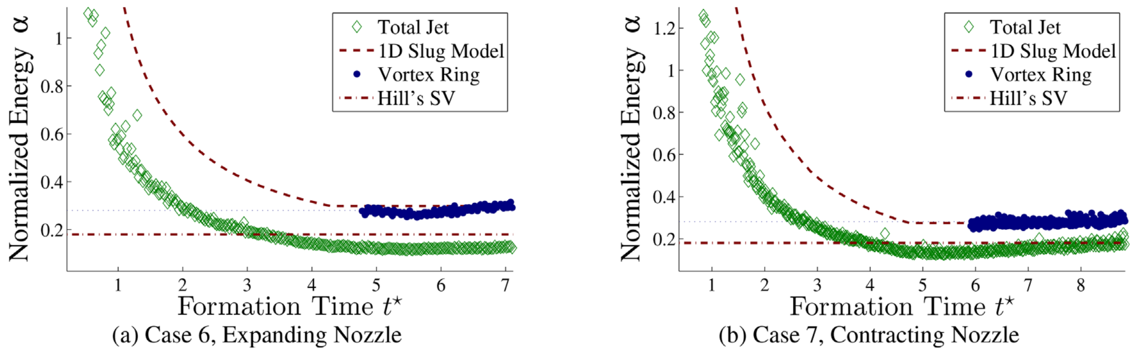

FIG. 22. Non-dimensional energy, α, vs formation time, as defined by (A2), for jets created with expanding and contracting nozzles. Experimental case 6 is shown in (a) and case 7 is shown in (b).

comparison of increased formation number from that study is complicated by the use of formation time definition (A5) which is defined by final ring scaling.

Experiments performed by Dabiri and Gharib[20] suggest that a converging nozzle radius will increase the formation number of the jet as high as 8. However, the volume flux program in that investigation was not compensated for the changing nozzle area so the converging nozzle radius also results in an accelerating jet flow. Therefore, the observed increase in formation number could just as likely be due to the acceleration of the feeding velocity, not the change in nozzle radius. Especially since the increase in formation number from that study is nearly identical to the increase seen with piston velocity acceleration here, case 5.

Figure 21 shows that the centerline velocity criterion still coincides with vortex ring pinch-off for starting jets with variable diameter nozzles. We also verify that the final ring configuration has not changed significantly from the static orifice nozzle case by plotting the final non-dimensional energy of cases 6 and 7 in Fig. 22. It can be seen that the decreasing radius jet (whose formation number is nearly identical to the formation number of the constant radius jet) has a final non-dimensional energy of $\alpha = 0.275$ which is very close to the non-dimensional energy of the jet expelled through the constant radius nozzle. Similarly, the energy of the increasing radius jet is $\alpha = 0.279$.

DATA AVAILABILITY

The data that support the findings of this study are available from the corresponding author upon reasonable request.

REFERENCES

[1]M. Gharib, E. Rambod, and K. Shariff, A universal time scale for vortex ring formation. J. Fluid Mech. **360**, 121 (1998).
[2]I. K. Bartol, P. S. Krueger, J. T. Thompson, and W. J. Stewart, Swimming dynamics and propulsive efficiency of squids throughout ontogeny. Integr. Comp. Biol. **48**, 720 (2008).
[3]I. K. Bartol, P. S. Krueger, W. J. Stewart, and J. T. Thompson, Hydrodynamics of pulsed jetting in juvenile and adult brief squid Lolliguncula brevis: Evidence of multiple jet 'modes' and their implications for propulsive efficiency. J. Exp. Biol. **212**, 1889 (2009).
[4]M. Sahin and K. Mohseni, The numerical simulation of flow patterns generated by the hydromedusa Aequorea victoria using an arbitrary Lagrangian-Eulerian formulation. AIAA Paper No. 2008-3715 (Seattle, WA, USA, 2008).
[5]M. Sahin and K. Mohseni, An arbitrary Lagrangian-Eulerian formulation for the numerical simulation of flow patterns generated by the hydromedusa Aequorea victoria. J. Comput. Phys. **228**, 4588 (2009).
[6]M. Sahin, K. Mohseni, and S. Colin, The numerical comparison of flow patterns and propulsive performances for the hydromedusae Sarsia tubulosa and Aequorea victoria. J. Exp. Biol. **212**, 2656 (2009).
[7]D. Lipinski and K. Mohseni, Flow structures and fluid transport for the hydromedusae Sarsia tubulosa and Aequorea victoria. J. Exp. Biol. **212**, 2436 (2009).
[8]J. O. Dabiri, S. P. Colin, K. Katija, and J. H. Costello, A wake-based correlate of swimming performance and foraging behavior in seven co-occuring jellyfish species. J. Exp. Biol. **213**, 1217 (2010).
[9]M. Gharib, E. Rambod, A. Kheradvar, D. J. Sahn, and J. O. Dabiri, Optimal vortex formation as an index of cardiac health. Proc. Natl. Acad. Sci. U. S. A. **103**, 6305 (2006).
[10]M. Krieg and K. Mohseni, Thrust characterization of pulsatile vortex ring generators for locomotion of underwater robots. IEEE J. Oceanic Eng. **33**, 123 (2008).
[11]J. Norbury, A family of steady vortex rings. J. Fluid Mech. **57**, 417 (1973).
[12]L. E. Fraenkel, Examples of steady vortex rings of small cross-section in an ideal fluid. J. Fluid Mech. **51**, 119 (1972).
[13]M. J. M. Hill, On a spherical vortex. Philos. Trans. R. Soc. A **185**, 213 (1894).
[14]K. Mohseni and M. Gharib, A model for universal time scale of vortex ring formation. Phys. Fluids **10**, 2436 (1998).
[15]M. Rosenfeld, E. Rambod, and M. Gharib, Circulation and formation number of laminar vortex rings. J. Fluid Mech. **376**, 297 (1998).
[16]M. Krieg and K. Mohseni, Modelling circulation, impulse and kinetic energy of starting jets with non-zero radial velocity. J. Fluid Mech. **719**, 488 (2013).
[17]M. Rosenfeld, K. Katija, and J. O. Dabiri, Circulation generation and vortex ring formation by conic nozzles. J. Fluids Eng. **131**(1), 091204 (2009).
[18]K. Mohseni, H. Ran, and T. Colonius, Numerical experiments on vortex ring formation. J. Fluid Mech. **430**, 267 (2001).
[19]P. Krueger, J. Dabiri, and M. Gharib, The formation number of vortex rings formed in a uniform background co-flow. J. Fluid Mech. **556**, 147 (2006).
[20]J. O. Dabiri and M. Gharib, Starting flow through nozzles with temporally variable exit diameter. J. Fluid Mech. **538**, 111 (2005).
[21]L. Pantzlaff and R. M. Lueptow, Transient positively and negatively buoyant turbulent round jets. Exp. Fluids **27**, 117 (1999).
[22]C. Marugán-Cruz, J. Rodriquez-Rodriquez, and C. Martinez-Bazán, Formation regimes of vortex rings in negatively buoyant starting jets. J. Fluid Mech. **716**, 470 (2013).
[23]P. Philippe, C. Raufaste, P. Kurowski, and P. Petitjeans, Penetration of a negatively buoyant jet in a miscible liquid. Phys. Fluids **17**, 053601 (2005).
[24]C. Marugán-Cruz, J. Rodriquez-Rodriquez, and C. Martinez-Bazán, Negatively buoyant starting jets. Phys. Fluids **21**, 117101 (2009).
[25]W. Lin and S. W. Armfield, Direct simulation of weak axisymmetric fountains in homogeneous fluids. J. Fluid Mech. **403**, 67 (2000).
[26]T. B. Benjamin, The alliance of practical and analytical insights into the nonlinear problems of fluid mechanics, in *Applications of Methods of Functional*

Analysis to Problems in Mechanics: Proceedings of the Joint Symposium IUTAM/IMU, edited by P. Germain and B. Nayroles (Springer-Verlag, New York City, NY, USA, 1976), pp. 8–29.
[27]P. H. Robert and R. J. Donnelly, Dynamics of vortex rings. Phys. Lett. A **31**, 137 (1970).
[28]P. H. Robert, A Hamiltonian theory for weakly interacting vortices. Mathematika **19**, 169 (1972).
[29]J. Norbury, A steady vortex ring close to Hill's spherical vortex. Proc. Cambridge Philos. Soc. **72**, 253 (1972).
[30]L. E. Fraenkel, On steady vortex rings of small cross-section in an ideal fluid. Proc. R. Soc. London, Ser. A **316**, 29 (1970).
[31]M. Shusser and M. Gharib, A new model for inviscid vortex ring formation. AIAA Paper No. 99-3805 (Norfolk, VA, USA, 1999).
[32]M. Shusser and M. Gharib, Energy and velocity of a forming vortex ring. Phys. Fluids **12**, 618 (2000).
[33]A. Friedman and B. Turkington, Vortex rings: Existence and asymptotic estimates. Trans. Am. Math. Soc. **268**, 1 (1981).
[34]B. Steinfurth and J. Weiss, Vortex rings produced by non-parallel planar starting jets. J. Fluid Mech. **903**, A16 (2020).
[35]T. Maxworthy, The structure and stability of vortex rings. J. Fluid Mech. **51**, 15 (1972).
[36]T. Maxworthy, Some experimental studies of vortex rings. J. Fluid Mech. **81**, 465 (1977).
[37]H. Lamb, *Hydrodynamics* (Dover, Mineola, NY, USA, 1945).
[38]D. G. Akhmetov, *Vortex Rings* (Springer-Verlag, New York City, NY, USA, 2009).
[39]I. S. Gradshteyn and I. M. Ryzhik, *Table of Integrals, Series, and Products* (Academic Press, San Diego, CA, USA, 2000).
[40]C. E. Willert and M. Gharib, Digital particle image velocimetry. Exp. Fluids **10**, 181 (1991).
[41]M. Raffel, C. E. Willert, and, and J. Kompenhans, *Particle Image Velocimetry* (Springer-Verlag, New York City, NY, USA, 1998).
[42]P. G. Saffman, *Vortex Dynamics* (Cambridge University Press, Cambridge, UK, 1992).
[43]T. T. Lim and T. B. Nickels, Vortex rings, in *Fluid Vortices*, edited by S. I. Green (Springer-Verlag, New York City, NY, USA, 1995), pp. 95–153.
[44]J. S. Marshall, "Inviscid Incompressible Flow, ch. Axisymmetric Vortex Flows," in *Inviscid Incompressible Flow* (Wiley-Interscience, New York, 2001), pp. 260–295.
[45]M. Krieg and K. Mohseni, On approximating the translational velocity of vortex rings. ASME J. Fluids Eng. **135**, 124501 (2013).
[46]W. C. Reynolds, D. E. Parekh, P. J. D. Juvet, and M. J. D. Lee, Bifurcating and blooming jets. Annu. Rev. Fluid Mech. **35**, 295 (2003).
[47]J. P. Sullivan, S. E. Widnall, and S. Ezekiel, Study of vortex rings using a laser Doppler velocimeter. AIAA J. **11**, 1384 (1973).
[48]D. W. Moore and P. G. Saffman, A note on the stability of a vortex ring of small cross-section. Proc. R. Soc. A **338**, 535 (1974).
[49]P. G. Saffman, The number of waves on unstable vortex rings. J. Fluid Mech. **84**, 625 (1978).